Facile Hydrothermal Synthesis of Copper Based Binary and Ternary Electrocatalysts for Efficient Water and Methanol Oxidation

By

Humaira Bibi

(Registration No: 00000331151)

A thesis submitted to the National University of Sciences and Technology,

Islamabad in partial fulfillment of the requirements for the degree of

Master of Science in Chemistry

Thesis Supervisor: Dr. Muhammad Adil Mansoor

Department of Chemistry,

School of Natural Sciences

National University of Sciences & Technology (NUST)

Islamabad, Pakistan

(2023)

THESIS ACCEPTANCE CERTIFICATE

Certified that final copy of MS thesis written by **Humaira Bibi** (Registration No. **00000331151)**, of **School of Natural Sciences** has been vetted by undersigned, found complete in all respects as per NUST statutes/regulations, is free of plagiarism, errors, and mistakes and is accepted as partial fulfillment for award of MS/M.Phil degree. It is further certified that necessary amendments as pointed out by GEC members and external examiner of the scholar have also been incorporated in the said thesis.

Signature: _____

Name of Supervisor: Dr. M. Adil Mansoor

Date: _____

Signature (HoD): _____

Date: _____10/08/2023_____

Signature (Dean/Principal): _____

Date: _____11/08/23_____

National University of Sciences & Technology

MS THESIS WORK

We hereby recommend that the dissertation prepared under our supervision by: Humaira Bibi, Regn No. 00000331151 Titled: Facile Hydrothermal Synthesis of Copper Based Electrocatalysts for Efficient Water and Methanol Oxidation be Accepted in partial fulfillment of the requirements for the award of **MS** degree.

Examination Committee Members

1. Name: PROF. MUHAMMAD ARFAN   Signature: _____

2. Name: DR. SHAHID IQBAL   Signature: _____

Supervisor's Name DR. M. ADIL MANSOOR   Signature: _____

_____
Head of Department

_7/8/23_
Date

COUNTERSINGED

Date: **07·08·2023**

_____
Dean/Principal

Dedication

To the Saviour of mankind

Prophet Muhammad (PBUH)

&

My beloved Parents

Whose prayers and affections are the source of strength for me in every step of my life and a sign of success for my bright future. Their efforts, devotion, love, and care cannot be repaid throughout the whole span of my life.

Acknowledgment

All praises to **ALLAH**, who is the only praiseworthy in the universe. He is the entire source of knowledge, guidance, and wisdom awarded to mankind. I thank **ALLAH,** the gracious and sympathetic that I have been able to undertake and complete my research work. All respect to **Holy Prophet Hazrat Muhammad (PBUH)** who have been forever a source of guidance.

I express my heartfelt thanks to my learned, reverend, and cooperative research supervisor **Dr. Muhammad Adil Mansoor**, Associate Professor, School of Natural Sciences, NUST, for his keen interest, advice, consistent encouragement, boosting my confidence and sympathetic attitude which were the real source of inspiration for me throughout my research work.

I am immensely grateful to **Dr. Shahid Iqbal**, **Dr. Muhammad Arfan**, (GEC members) for their teaching, and valuable recommendations and for providing me required facilities during my research work. I am thankful to Principal **Dr. Rashid Farooq** and HoD Chemistry **Dr. Azhar Mahmood** for ensuring the availability of a conducive research environment.

I am grateful to the School of Natural Sciences (SNS) at NUST for facilitating me in thesis work.

I wish to offer my thanks to my seniors and all lab fellows for their co-operation and for providing me with a friendly environment. I am indebted to my friends for standing by my side throughout this time and providing me with the emotional support I needed. I thank my parents deeply for their trust, support, and love. I will not forget to extend my thanks to my sisters and brother for being the best listener and giving me the support, I needed for the completion of this report.

My cordial thanks to my uncles, brothers, and sisters for their co-operation, and moral support throughout my research.

Humaira Bibi

Contents

Abstract

The search is on for highly efficient, catalytically active materials that can produce and store sustainable fuels, particularly H_2 gas. Because fossil fuels are running out and have a negative effect on the environment energy ,professionals are investigating alternative fuel generation techniques that are sustainable, cost-effective, eco-friendly, and easy to store. H_2 gas is considered the best option for energy storage, as it emits zero carbon and is renewable. However, its production requires catalysts, and recent advancements in the field have focused on using transition metal-based materials for electrochemical catalysis. This study develops copper-based composites that work well as electrocatalysts for the oxidation of water and methanol via hydrothermal synthesis. The material's structure and composition were analyzed using X-ray diffraction, Scanning electron microscopy, Electron dispersive spectroscopy and Transmission electron microscopy . The optimized catalytic samples were then used to evaluate their efficiency and stability in electrochemical water and methanol oxidation. Since being successful, these catalysts could be employed on an industrial scale, leading to an increased production of renewable hydrogen to meet global energy demand.

Keywords: Water oxidation, Electrocatalyst, H_2 generation, Methanol oxidati

Chapter 1: Introduction

The tremendous rise in population in the twenty-first century has accelerated the demand for greener, more powerful energy sources. [1]. Both the global energy crisis and environmental problems are becoming more serious . [2]. The energy needs of business and daily life are rising quickly as more and more complex technology is being used in modern society [3]. Modern civilization's employment of more advanced technology has resulted in a rapid rise in the amount of energy needed for both daily life and business [4]. Due to the climate change brought on by the combustion of fossil fuels and the speeding up of industrialization, a shift in the global energy paradigm is necessary. [2].

Among the most promising energy sources biomass, geothermal, wind, solar energy and tides are the most auspicious sources of energy. In addition, energy conversion devices for efficient and emission-free conversion of fossil fuels and renewable energy sources into useful energy products are essential for the modern era. Fuel cells, due to their high efficiency, non-moving parts, non-pollutant products, and side products, are a preferable option compared to gas and diesel engines, wind turbines, nuclear and hydroelectric power plants, and other energy conversion devices [4, 5]. Depending on the required temperature, there are two types of fuel cells: High-temperature fuel cells and low-temperature fuel cells. A low-temperature fuel cell, due to its low-temperature requirements and higher CO tolerance, is a better option than a high-temperature fuel cell. Oxygen reduction reaction (ORR), carbon dioxide reduction reaction (CRR), hydrogen evolution reaction (HER), oxygen evolution reaction (OER), methanol oxidation reaction (MOR), urea oxidation reaction (UOR), and ammonia oxidation reaction (AOR) are a few of the electrochemical reactions that take place in fuel cells.

1.1 Problem Statement

The creation of renewable energy sources is crucial for reducing CO_2 emissions and tackling global warming since traditional nonrenewable fuels have contributed to air pollution. The primary sources of renewable energy today include nuclear, geothermal, biomass, wind, and water. These sources must overcome their shortcomings, which include high costs and low efficiency, to be sustainable. Scientists are working to create dependable, recyclable, and ecologically acceptable renewable energy sources to fulfill energy demands and improve the efficacy of recently found storage systems. Renewable energy technologies are discontinuous power sources because of their cyclical and seasonal variations. To fulfil the continued need for power, research has focused on preserving the existing fossil fuel sources and enhancing their efficiency. To satisfy the demand for a constant supply of energy, researchers are also focusing on preserving the present fossil fuel sources and enhancing the efficiency of renewable energy storage. To reduce atmospheric CO_2 emissions from conventional, non-renewable fuels, limit the rate of global warming, and build sustainable societies for the next generation, green, renewable energy sources must now be developed. The main operating sources of renewable energy today include wind, water, solar, biomass, geothermal, and nuclear energy. (Figure 1).

Figure 1. Some important renewable energy sources.

Some technological and economic barriers need to be removed to convert these energy sources into a commercially viable power source. Scientists are always attempting to replace conventional fossil fuels with dependable, recyclable, and ecologically friendly renewable sources to fulfil the world's energy demands. Energy researchers must also balance safeguarding current fossil fuel power sources, developing new renewable energy sources, and enhancing the efficiency of newly discovered renewable energy techniques' storage capabilities. In this search ,transition metal-based oxides are widely used but the problem with their use is their low efficiency, high over potential, low current density, less stability, and high susceptibility to corrosion, sluggish OER kinetics, and CO adsorption which renders the activity of catalyst in the case of methanol oxidation.(Figure 1.1) So, the focus of this study revolves around minimizing/solving all these problems.
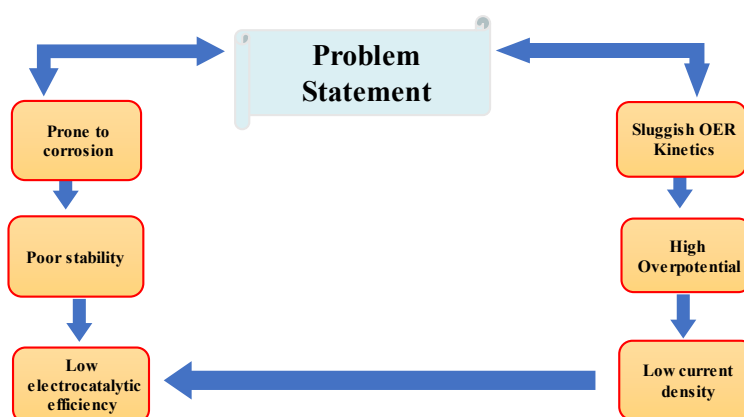
Figure 2. Problem Statement

1.2 Technologies for Renewable Energy

Technologies that use renewable energy are vulnerable to cyclical and seasonal fluctuations. These are therefore thought of as sporadic power sources. The way we live now requires a steady flow of energy, which is something that currently available renewable energy sources cannot deliver. Energy storage systems must be connected to these renewable energy production systems to store additional energy produced during peak energy production times for usage during low production periods. Numerous well-known methods and innovations, including mechanical and thermal

conversion, batteries, and chemical bonding, can be used to store renewable energy. Perhaps the oldest technology still in use today is hydropower, which employs mechanical energy conversion and storage. The basic concept of this pumped hydroelectric energy storage device is simple. The water is forced via electrically powered turbines from the area of low reservoir towards the high reservoir, where it is stored as potential energy and is forced to return to the low reservoir when power is required, transforming potential energy into kinetic energy. Following that, this kinetic energy is used to replenish the electricity. Since it is not practical to recharge the water reservoir every day, this method fully empties it. However, it extends beyond the discussion's focus on producing consistent energy that is compatible with demand. This renewable energy may be stored as a backup plan to fulfil an unforeseen need for electricity during hours of need.

The second option, solar thermal technology, is the ideal substitute for natural gas. Sunlight is utilized to heat liquids like water in this type of thermal storage; on a small scale, it may even be used to heat a home and supply hot water. If they are properly regulated, they may be utilized in bigger structures and even in enterprises where diverse processes call for the utilization of heat and vapors. Effective use of this technology might reduce utilization. The third option for renewable energy technologies includes batteries. Although batteries are often used nowadays, they are still not very good at storing the energy produced by solar or wind power. These batteries' worse efficiency can be attributed to lower gravimetric and volumetric energy density. The issue of energy density of battery is less significant when focusing on smaller devices like smartphones or laptops. Large-scale applications like electric cars are significantly impacted by these batteries' reduced energy density. Additionally, the battery's components gradually degrade as it is being charged. They discharge, which causes a continuous loss of storage capacity and, as a result, the lowest level of durability for the system. Therefore, paying for the battery throughout the course of these PV modules' normal lifetime is no longer financially feasible.

The only energy storage strategy available to us is the usage of chemical bonding. In this process, an endergonic reaction is driven by energy. The byproducts of the reaction can be retained and recombined when required to create energy in a controlled way. The endergonic mechanism used for this energy storage purpose involves splitting water into hydrogen and oxygen.[5] It works the same way that plants do to split the water. Sunlight is used by plants to break down water into its constituent components, which are then mixed with carbon dioxide from the atmosphere and previously formed hydrogen equivalents to produce carbohydrates. The entire process may be artificially reproduced using methanol for the aim of storing energy. Because current industries have the means for storing and distributing H_2, using H_2 directly as fuel is more practical [6]. However, current industrial methods and processes are inefficient at supplying the energy required to combine H_2 and CO_2 into methanol. What are the possible techniques for isolating the different gases that make up water? Water can be broken through thermochemical water splitting, photobiological water splitting, thermolysis, electrolysis, and photo electrolysis, among other ways.[7]

For the thermolysis of water, higher temperatures, between 2000 and 2500 ° C, are needed. For this high-temperature heating approach, an affordable heating source and materials capable of withstanding high temperatures are needed.[8] The only energy source that can be used in this process is geothermal energy because it is a cheap source of heat. The thermochemical water splitting process takes place at actual temperature. It is nevertheless reliant on certain chemical cycles. Due to the caustic nature of the chemicals employed in the process and the broad usage of these chemical facilities, designing is time-consuming. The photobiological water splitting technique divides water into its component gases using green algae and cyanobacteria as well as light[9]. The scope of use of this approach is limited by the extremely slow processing speed. Electrolysis is still the final stage of water splitting that is the most efficient. There is still more work to be done in this area to raise the efficiency of electrolyzers while maintaining their cost as

low as feasible in order for them to achieve efficiency comparable to conventional non-renewable fossil fuels [10].
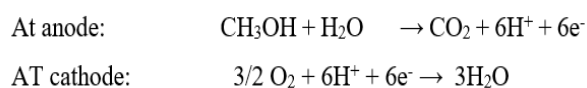
1.3 Types of Fuel Cell

One type of electrochemical device is a fuel cell, with its cathode and anode electrodes submerged in the electrolyte. The properly constructed electrolyte can only let ion transport; electrons are not permitted. A fuel cell's reported energy efficiency typically ranges from 40 to 60%.According to the kind of electrolyte, operating temperature, efficiency, fuel utilized, and power output, the fuel cell has been categorized into several types[11].

  i. Direct methanol fuel cell

 ii. Proton exchange membrane fuel cell

iii. Phosphoric acid fuel cell

 iv. Molten carbonate fuel cell

  v. Alkaline fuel cell

 vi. Solid oxide fuel cell

1.3.1 Direct Methanol Fuel Cell

In DMFC, methanol is used as fuel, and by oxidizing it, chemical energy that has been stored is transformed into electrical energy. High power and energy density are this fuel cell type's key As benefits. an illustration of a low-temperature fuel cell. Figure 1.2.[13, 14].
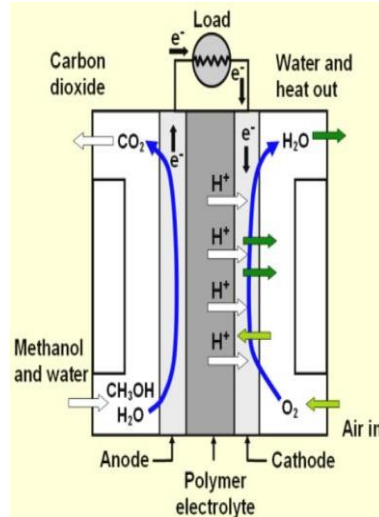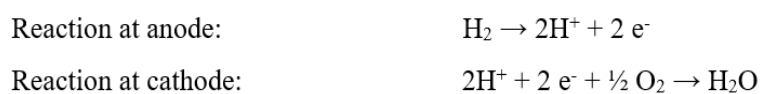
$$At\ anode: \qquad CH_3OH + H_2O \quad \rightarrow CO_2 + 6H^+ + 6e^-$$
$$AT\ cathode: \qquad 3/2\ O_2 + 6H^+ + 6e^- \rightarrow\ 3H_2O$$

Figure 1.2: Schematic representation of DMFC [14].

1.3.2 Proton Exchange Membrane Fuel Cell

In a PEMFC, electrochemical conversion of chemical energy into electrical energy is through smooth proton (H^+) passage from anode to cathode over a polymeric membrane. It is a low-temperature fuel cell that tolerates CO well, has little electrolyte management requirements, and has no corrosion from solid electrolyte. Methane may be converted into fuel-grade hydrogen via steam reforming. Figure 1.2

At anode: $H_2 \rightarrow 2H^+ + 2\ e^-$

At cathode: $2H^+ + 2\ e^- + \frac{1}{2}\ O_2 \rightarrow H_2O$
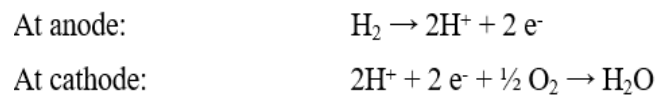
In a PEMFC, electrochemical conversion of chemical energy into electrical energy is performed via smooth proton (H+) passage from anode to cathode over a polymeric membrane. It is a low-temperature fuel cell that tolerates CO well, has little electrolyte management requirements, and has no corrosion from solid electrolyte. Methane may be converted into fuel-grade hydrogen via steam reforming. Figure 1.3[12].
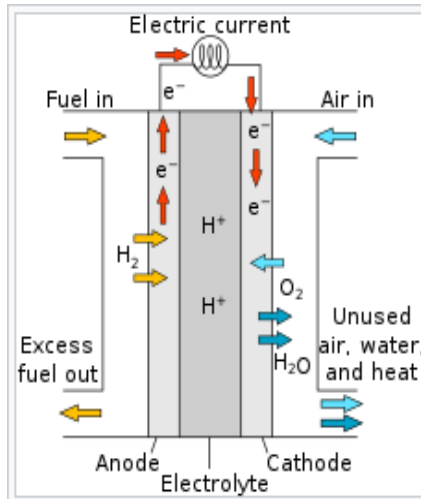
Reaction at anode: $H_2 \rightarrow 2H^+ + 2\ e^-$

Reaction at cathode: $2H^+ + 2\ e^- + \frac{1}{2}\ O_2 \rightarrow H_2O$

7

Figure 1.3 : Illustrative description of PEMFC [12]

1.3.3 Phosphoric Acid Fuel Cell

Low temperatures enable this fuel cell to operate. when oxygen is reduced at the cathode and hydrogen is oxidized at the anode and the presence of an electrolyte of phosphoric acid, an electrode reaction takes place. It produces a reasonable amount of heat, has a long lifespan, and a predisposition to create high power densities. It also has better CO tolerance than PEMFC. Figure 1.4 [15].
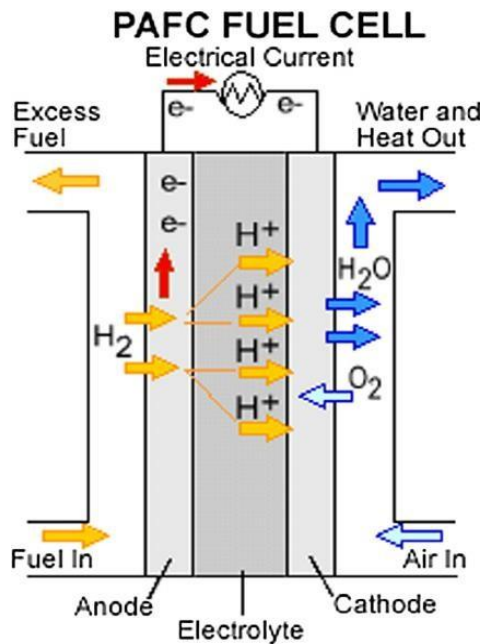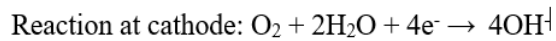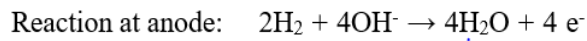
Reaction at anode: $2H_2 + 4OH^- \rightarrow 4H_2O + 4\ e^-$

Reaction at cathode: $O_2 + 2H_2O + 4e^- \rightarrow 4OH^-$

8

Figure 1.4: Schematic illustration of PAFC [15].

1.3.4 Molten Carbonate Fuel Cell

Temperatures of 650 °C or more are required for high-temperature fuel cells like this one. In the presence of a molten carbonate electrolyte, anode hydrogen oxidation and cathode carbon dioxide reduction occur. The silent properties of MCFC allow it to provide high-quality, inexpensive heating. Figure 1.5 [16].

At anode: $H_2 + CO_3^{-2} \rightarrow H_2O + CO_2 + 2\ e^-$

At cathode: $CO_2 + \frac{1}{2} O_2 + 2e^- \rightarrow CO_3^{-2}$
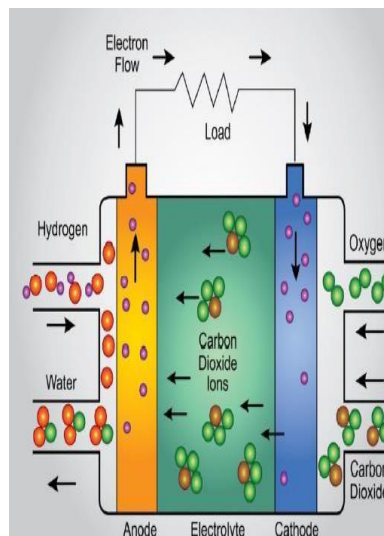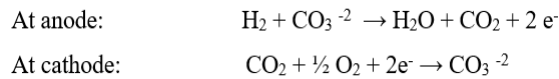
Figure 1.5: Schematic diagram of MCFC [16]

1.3.5 Alkaline Fuel Cell

It serves as an example of a low-temperature fuel cell in which water is created by the reaction of H^+ and OH^- ions in the electrolyte (KOH) and at cathodic electrode, oxygen is reduced, while at anodic electrode, hydrogen is oxidized. They only get oxygen from purified air since they are particularly vulnerable to CO2 poisoning. Figure 1.6 [15].

Reaction at anode: $2H_2 + 4OH^- \rightarrow 4H_2O + 4\ e^-$

Reaction at cathode: $O_2 + 2H_2O + 4e^- \rightarrow 4OH^-$

9
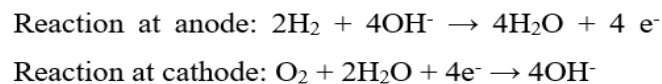
Figure 1.6: Illustrative description of AFC [15]

1.3.6 Solid Oxide Fuel Cell

It serves as an illustration of a 70% efficient high-temperature fuel cell. While oxygen reduction

occurs at the cathode, hydrogen oxidation at the anode. Figure 1.7 [16].

Reaction at anode: $2H_2 + 2O^{-2} \rightarrow 2H_2O + 4 \ e^-$

Reaction at cathode: $O_2 + 4e^- \rightarrow 2O^{-2}$
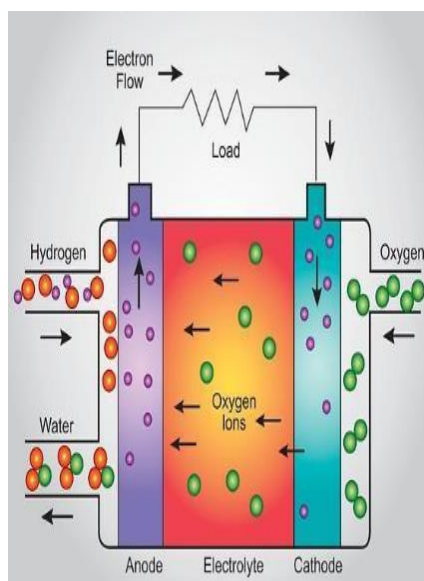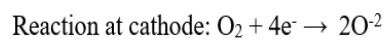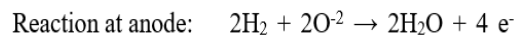
Figure 1.7: Schematic representation of SOFC [16].

1.4 Electrochemical Reactions of a Fuel Cell

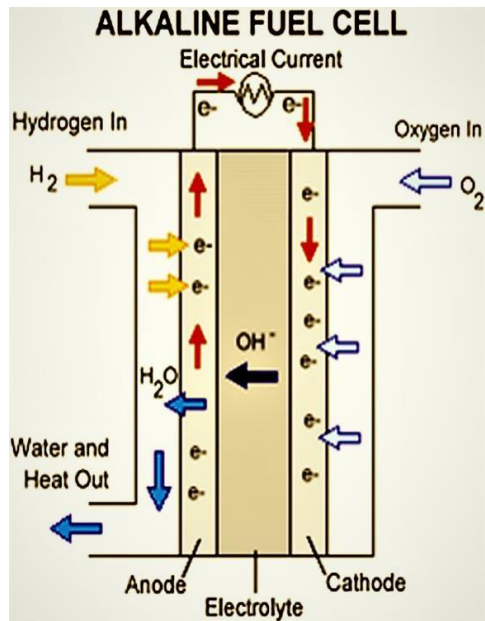Important electrochemical reactions in an acidic/alkaline fuel cell include the following: Methanol oxidation and oxygen evolution are instances of anodic processes, whereas hydrogen evolution, oxygen reduction, and CO_2 reduction are examples of cathodic reactions. Conducting anodic processes like MOR and OER may be done in acidic, neutral, or alkaline conditions. Although analyte oxidation occurs at low onset and peak potential, reaction intermediates are easily oxidized due to their weak binding and abundant availability of oxygen-containing groups, there are an increasing number of electroactive sites available, electron and ion diffusion is facilitated, and the material is more stable, so an electrocatalyst performs better in an alkaline medium[17].

1.4.1 Oxygen Evolution Reaction

$$H_2 O \rightarrow H_2 + \tfrac{1}{2} O_2 \qquad 1.23 \text{ V vs. RHE}$$

Basic/Neutral media	Acidic media
$M + OH^- \rightarrow MOH$	$M + H_2O \rightarrow MOH + H^+ + e^-$
$MOH + OH^- \rightarrow MO + H_2O$	$MOH + OH^- \rightarrow MO + H_2O + e^-$
$2MO \rightarrow 2M + O_2$	$2MO \rightarrow 2M + O_2$
$MO + OH^- \rightarrow MOOH + e^-$	$MO + H_2O \rightarrow MOOH + H^+ + e^-$
$MOOH + OH^- \rightarrow M + O_2 + H_2O$	$MOOH + OH \rightarrow M + O_2 + H^+ + e^-$
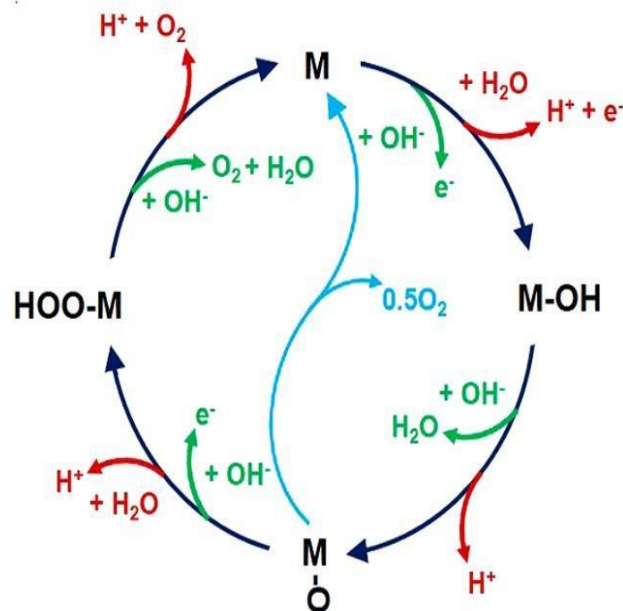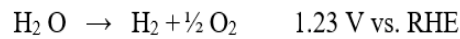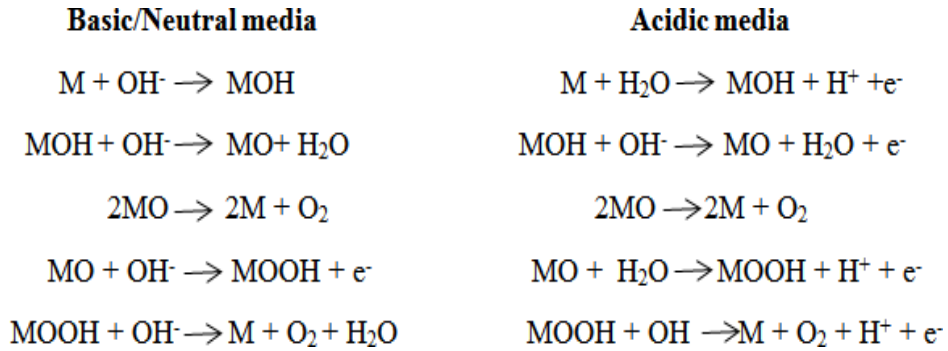
Figure 1.8: Reaction steps of OER in an acidic and basic media [19].

1.4.2 Methanol Oxidation Reaction

During the anodic process of oxidation of methanol, which also releases protons, electrons, and CO_2, CH_3OH (aq) is oxidized at an anode surface. Both protons and electrons take part in the process of oxygen reduction on cathode surface via diffusion via membranes and external circuits, respectively. Each phase of the reaction is listed in Figure. 1.9 [20].

$CH_3OH + H_2O \rightarrow CO_2 + 6H^+ + 6e^-$ $E^0 = 0.016$ V (vs. RHE)   (Anode reaction)

$3/2\ O_2 + 6H^+ + 6e^- \rightarrow 3H_2O$ $E^0 = 1.229$ V (vs. RHE)   (Cathode reaction)

$CH_3OH + 3/2\ O_2 \rightarrow CO_2 + 2H_2O$ $E^0 = 1.213$ V (vs. RHE)   (Overall reaction)

Figure 1.9: MOR reaction steps [20].

1.5 : The criteria for measuring the activity of electrocatalytic water

oxidation

The electrochemical testing of as-fabricated catalysts is performed on a three-electrode electrochemical setup coupled with an electrochemical workstation that is computer-controlled. Galvanostatic and potentiostatic studies for a range of electrocatalytic processes can be carried out at this workstation. The electrode where the reaction of 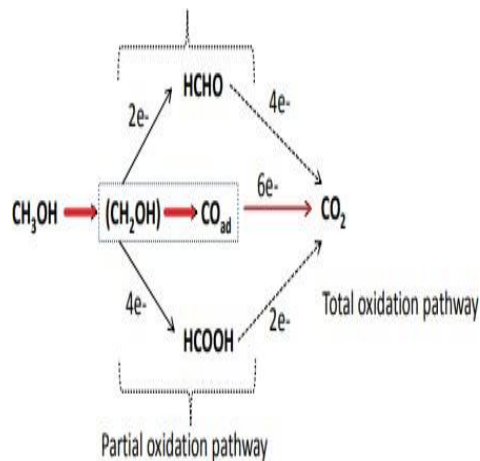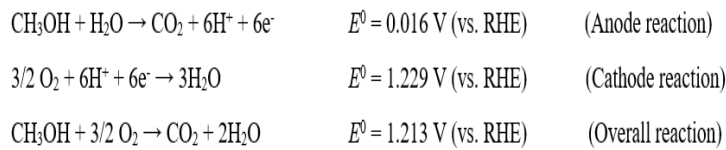interest is occurring in this three-electrode arrangement is referred to as working electrode, and it is normally the electrode with the as-prepared loaded water oxidation catalyst. The counter electrode that is used most is platinum wire. The two reference electrode types used mostly in the three-electrode configuration are the standard calomel electrode and another one is Ag/AgCl electrode. The polarization curve is the main analytical tool used to check the response of the electrochemical catalysts . Both linear sweep voltammetry (LSV) and cyclic voltammetry (CV) are tools to record polarization curves. By scanning a cycle within a predefined range of potential (either positive or negative, or between positive and negative big voltage range), the method of cyclic voltammetry is used to measure current as a response. There is no cycle-like scan of the voltage with linear sweep voltammetry [21].

$$E_{vs}RHE = E_{vs}Reference + 0.059(pH) + E°Reference$$

Here, $E°$ Reference denotes the reference electrode's standard thermodynamic potential whereas E_{vs} Reference denotes the experiment's potential.

The factors to assess water and methanol oxidation reaction are:

1. **Current density (j)** .

 From the polarization curves, the area normalized current, or current density (j), is obtained. Dividing current obtained in the polarization curves by electrode's geometric area is the value known as the current density (j).

$$J= Current(mA)/Geometric\ Area\ of\ electrode\ (cm^2)$$

2. Onset Potential

The starting point of the desired reaction is indicated by the term "**onset potential**" in the polarization curves. According to the current value of OER in our case, it is the point on the curve when the curve starts to increase. It is often taken directly from the LSV or CV graph.

3. Overpotential

The term "**Overpotential**" describes the amount of additional voltage required over and above the normal thermodynamic potential of oxygen to develop oxygen by water splitting. The common measurement threshold for water splitting applications is 10 mA cm^{-2} [8]. This potential value is known as overpotential (η_{10}) and is represented by the following for a decade of current density.

$$\eta_{10} = E_{RHE} - 1.229$$

4. The Tafel equation

It is used to evaluate the rate-setting step in an electrochemical reaction and determine the estimated length of the reaction process. A specific electrocatalytic process's charge transfer kinetics is described in detail by the equation. The exchange current density is another activity metric that may be calculated using the Tafel equation. The slope of the Tafel equation may be used to determine the volume of charges transferred during an electrochemical process [29]. The simplest way to explain the Tafel equation is as follows:

$$\eta = a + b\log j$$

In this example, "a" signifies the intercept value, "j" shows current density, and "b" represents. Tafel slope

5 Electrochemical Impedance Spectroscopy

This is one technique for determining the impedance of the system. Its measurement provides

values for charge transfer resistance and solution resistance, which are denoted by R_{ct} and R_s[22], respectively. Simply fitting the Nyquist plot data with the most basic Randle's circuit yields these results.

5. Durability

The durability of the catalyst is evaluated by applying either a constant bias or constant current for an extended period. A catalyst is considered stable if it can sustain a particular potential or j value over a lengthy period. Chronopotentiometry (durability at constant current value) and chronoamperometry (durability at constant bias) are the names of these tests.

6. Faradic efficiency

It is another measure of electrocatalytic activity, obtained by counting the number of electrons that are delivered from the anode through an external circuit during the electrochemical process. By contrasting the amounts of O_2 generated theoretically and empirically, the Faradic Efficiency is also calculated. However, in principle, it can be predicted from the electrode surface area, current density, and time of the electrolysis. The evolved O_2 is determined in the experiment using Gas Chromatography[23].

7. Double-layer capacitance

It measures the electrochemically active surface area, and hence it is a valuable way to characterize the intrinsic electrocatalytic property of various materials. To determine the double-layer capacitance through CV in two steps, a current response of the material in the capacitive region is determined through several CV scans, and (b) in the second step, the curve is linearly fitted. The double layer capacitance can also be measured using electrochemical impedance spectroscopy. [24].

8. Exchange Current Density

An illustration of the material's electrocatalytic process at equilibrium is exchange current density (J_0). It may be estimated through the Tafel equation by supposing zero overpotential. [25] An exchange current dense material accelerates the process by lowering the activation energy barrier.

$$\eta = a + b \log \ J/J_0$$

η is overpotential (mV) while "a" represents surface area of electrode (cm^2) "b" is Tafel slope (mV/dec) and "j" represents current density (mA/cm^2).

1.6 Research Objectives

Recent investigations and kinetic assessments in the disciplines of electrochemical (EC) water and methanol oxidation indicate that catalysts accelerate their oxidation. Additionally, catalysts can aid in lowering overpotential values for the specific reaction. The two half-reactions that make up this reaction are the Oxygen Evolution Reaction (OER) and the Hydrogen Evolution Reaction (HER). Due to its complex and lengthy kinetics, OER is thought to be the more important process. The development of catalysts that might accelerate electrocatalytic water oxidation processes is the major objective of this thesis study. The oxygen gas produced by the water-splitting process is extensively employed in the fuel industry.

While HER works best in acidic media, the OER step of electrochemical water splitting performs best in alkaline media. The most efficient OER catalyst at present, needing the least amount of overpotential, is expected to be platinum metal. On the other hand, RuO_2 and IrO_2 are effective electrocatalysts, but they are quite expensive. Investigating alternatives to these precious metal oxides that are as effective and stable has been a major focus of research. Perovskites, chalcogenides, and transition metal oxides have all been investigated as prospective replacement electrocatalysts with outstanding electrocatalytic activity during the past 10 years. The most thoroughly studied and effective metals for electrocatalytic water splitting are nickel and copper.

In this research project, the copper-metal oxides and their composites will be prepared by hydrothermal method. The main objectives of this research work are to produce cost-effective and green alternatives to precious metal catalysts so that the as-produced catalysts can have low overpotential, high efficiency and appreciable stability to have their industrial-scale applications in the future to produce renewable fuels (Figure 1.9).
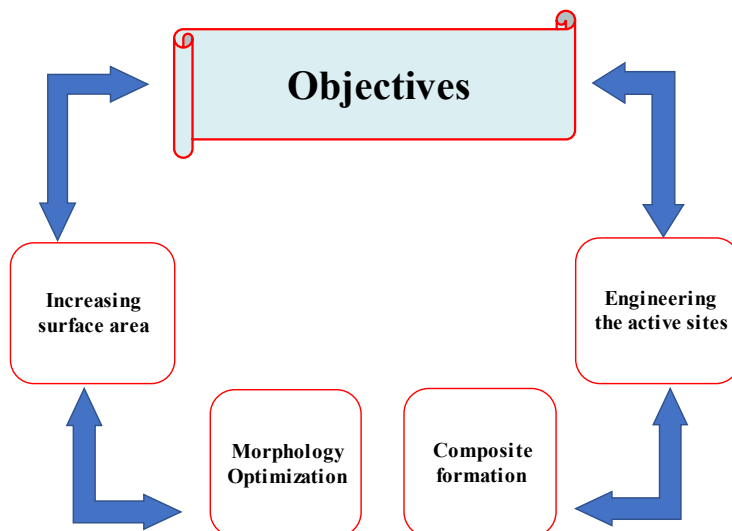

Figure 2.0 :Objectives of Research

Chapter 2   Literature Review

2.1 Literature Survey for Oxygen Evolution Reaction

Without using fossil fuels or emitting greenhouse gases, electrochemical splitting of water has been advocated as a practical solution to the world's expanding needs of energy. [26].This is due to the efficient creation of H_2 and oxygen (O_2) via electrochemical water splitting [27], [28], [29],[30], [31],[32].Without an electrocatalyst, the OER process often exhibits substantial overpotential and efficiency losses throughout the water-splitting process. Noble metal-based catalysts have great electrocatalytic activity in an acidic media because active sites are accessible, and they are stable. In comparison to Pd, Rh, and Pt, Ru and Ir are possible OER candidates among the noble metals. Although gold and osmium also exhibit better activity than ruthenium, their instability prevents practical use. Noble metal oxides are more stable than metallic forms, especially in basic media. Additionally, the increased electrocatalytic activity of these materials is greatly aided by noble metal alloys, hybrids with stable and conductive supports, and various morphologies, including three-dimensional structures, core-shell architecture, and layered double hydroxides. However, they are not used widely because of their instability, high cost, and sluggish kinetics. Transition metal-based electrocatalysts are effectively utilized for OER in an alkaline media due to less cost, availability, and strong catalytic activity brought on by changing oxidation states [33], [34], [2]. Examples of these TMs include oxides, [35], [36], [37], [38], [39],(oxy)hydroxide, [40], [41, 42], [43] sulphides [43, 44], [44]and phosphides [45], [46] etc.

The most extensively researched and most promising class of materials for electrocatalysis and electrochemistry are metal oxides, particularly transition metal oxides. It is because metal oxides have so many benefits. Materials made of metal oxides have well-controlled crystallographic, surface, and structural characteristics. Several of them have great aqueous stability and are non-

toxic. It is simple to modify and functionalize metal oxides through bulk doping or surface modification. [47]

Transition metal oxides and hydroxide are potential OER candidates in the case of non-noble metal electrocatalyst, and inserting stable and conductive support, such as CNTs, rGO, GO, PANI, etc. within the electrocatalyst is an effective technique to increase the OER. Using a double step solution method, Liang and colleagues created the Co_3O_4/N-Graphene composite in 2011. They subsequently tested it for OER activity. Due to the stronger link that formed between rGO and Co_3O_4 NPs because of the N content, which increases the efficiency of electron transport, a composite of N-rGO and metal oxide performed better than Co_3O_4 NPs. Due to its low onset potential and persistently steep Tafel slope, the Co_3O_4/N-rGO electrocatalyst displays excellent activity [68].

In 2011, Liang and coworkers developed the Co_3O_4/N-Graphene composite using a two-step solution technique. They next examined it in an alkaline media for OER activity. A composite of N-rGO and metal oxide outperformed Co_3O_4 NPs due to the stronger bond that formed between the two materials because of the N component, which boosts the efficiency of electron transport. The Co_3O_4/N-rGO electrocatalyst exhibits outstanding activity due to its low onset potential and persistently steep Tafel slope.[48]

In 2011, Peng and coworkers demonstrated performance of heteronanosheet-based bifunctional electrocatalysts $NiO-Ni_3S_2$/NF having the lowest Tafel value (75 mV dec. $^{-1}$), which points to a noticeably smoother path for $NiO-Ni_3S_2$/NF throughout the OER process.[49]

Jiang, et al. produced the 500-Ni/ WOx/NF-3 in 2021 . The optimum Ni/WOx/NF showed excellent OER performance with an overpotential of 395.7 mV at 100 mA cm^{-2} .Additionally, the Ni/WOx/NF can operate at a lower cell operating voltage (1.54 V) at 10 mA cm^{-2}[50].

Sun et al. produced a Co doped Cu_2S on copper foam (CoCu_2S/CF) using in situ hydrothermal sulfidation to serve as effective and reliable electrocatalyst for alkaline OER. It requires overpotential as low as 298 to afford 20 mA cm^{-2} in 1.0 M KOH [51].

Wu et al. in 2022 constructed Nickel cobalt hydroxide nanosheets directly on nickel coated copper oxide nanowires to produce a highly active hierarchical core-shell nanoarray of NiCo/Ni/CuO/CF. which showed negligibly small Tafel slopes of 37.9 mV dec1 and low overpotential of 246 mV at 10 mA cm^{-2}. According to extensive study, the distinctive nanowires design with the highly conductive nickel layer has been demonstrated to improve the active sites exposure and speed up the overall reaction[52].

Zhang et al. generated stanus and iron based oxyhydroxides and sulfides (SnFeS$_x$O$_y$/NF) in 2023 by using a solvothermal procedure that results in the heterostructure formation between the sulphides and oxyhydroxides. It exhibits 281 mV over potential at 100 mA cm^{-2} for the OER [53]. Li et al. successfully synthesized the bimetallic sulphides Ni$_3$S$_2$/CoS$_x$ that were intended to serve as OER catalyst and showed a low overpotential of 226 mV. [54].

Zhang et al. 2022 devised and applied a straightforward one-step method to produce the bimetallic silver-nickel sulphides heterostructures as extremely efficient OER catalysts with 260 mV overpotential at 10 mA/ cm^2 [55].

Fan and coworkers in 2022 produced a variety of binary metal sulphides with two-dimensional (2D) well defined nanosheet structures by utilizing a single step electrodeposition approach for OER which required 243 mV overpotential at 10 mA cm^{-2} current density. Its mechanism depends on the special 2D nanosheet topologies and Fe inclusion[56]

2.2 Literature Survey for Methanol Oxidation Reaction

Noble metals, like Pt, Ru, Rd are state-of-the-art components for MOR in acidic environments. Metal alloys, such as Pt metal with Ru incorporation, demonstrate greater MOR activity due to a higher tendency for OH$^-$ adsorption than single metal. The addition of other metals including Pd, Rd, Co, Ni, and Cu as well as the provision of a mesoporous conductive substrate with a sizable surface area further boosts the material's electrocatalytic performance due to a synergistic effect.

In 2018,the borohydride reduction procedure was used by Pattanayak, P., et al. to produce Cu_2O/PPyeGO which showed a peak current density of 300 mA cm^{-2} at 0.68 V.[57]

In 2010, Wang et al. used a simple reduction process to create the Pd-Co/C anode catalyst and adjusted the Co percentage before testing for MOR in an alkaline solution. The electrocatalyst displays 11 mA/cm^{-2} current density at 0.8 V and is supported by Pd-Co (8:1) and CNTs, resulting in a mesoporous structure with a wide surface area that is defect-rich. [58]

Pt-Ru nanowires were first developed in 2011 by Li et al., who used a soft template technique to regulate the size of the nanowires. By reducing metal ions with an ideal dosage of a reducing agent, 2D Pt-Ru NWRs (3.0 0.5 nm) were obtained. The optimized Pt-Ru NWRs' (0.4 g) current density response was much higher than others. Additionally, the electrocatalytic behaviour of Pt-Ru NWRs with varying amounts of Pt and Ru was examined. Pt-Ru (1:1) had the greatest activity, supplying 30.95 mA/cm^2 at 0.7 V [59].

Asgahri et al. (2012) examined the methanol oxidation propensity of Glassy Carbon Electrode (GCE) deposited on nickel cobalt alloy in 4:1 using CV, CA, and EIS. The effects of methanol concentration, solution temperature, and precursor ratio were also investigated in the electrochemical experiments. The modified Ni-Co electrode displays improved catalytic activity 0.821 A/cm^2 current density at 1.72 V (vs. RHE)[60].

In 2013, Raoof et al. used the potentiostat method to drop cast $Ni(OH)_2$ onto the surface of GCE. Electrochemical testing reveals the effects of scan rate, methanol concentration, and the Ni^{+3}/Ni^{+2} redox behavior. At higher concentrations, methanol, and Ni (III) have a substantial electrocatalytic interaction, whereas at lower concentrations, the MOR was diffusion controlled. By decreasing the reaction overpotential, MOR process moves more swiftly after producing Ni(III) on the electrode surface during the positive potential sweep [61]

In 2014, Das et al. employed a non-platinum $NiCo_2O_4$-rGO composite for MOR in an alkaline

environment that was inexpensive and practical. It displays the oxidation peak at a lower potential with a higher current density. The better electrocatalytic performance is due to the combined efforts of rGO and $NiCo_2O_4$ nanoparticles. [62]

In 2015, Li and associates solvothermally created the CNTs-supported Pt-CoP electrocatalyst and studied it for MOR. Due to the modification of CoP nanoparticles, Pt particle size is decreased, but EASA is improved because of the close relationship between CoP and Pt. In terms of electrocatalytic performance, the improved Pt/4%CoP/CNTs catalyst beats all other synthetic materials, giving a current density that is six times greater (1600 mA/mg) and more stable than traditional Pt-based electrocatalysts[63].

Iron-nickel nanoparticles (Fe-Ni NPs) with core shell-like properties were generated in an aqueous solution under ambient conditions utilizing a straightforward multistep synthetic process in 2016, according to Stephanie and colleagues. The response of current density continuously grows from 0.2 M to 2.0 M of methanol molarity. The catalyst as-prepared yields of 48 mA/cm^2 current density 1.58 V [64].

In 2017, Mehek et al. examined the methanol oxidation capability of cuboid shaped Co-BDC MOF/GO composites produced by solvothermal methods. In a solution of 3 M CH_3OH/IM KOH, the 5 wt % GO composite produces 0.0291 A/cm^2 current density at 1.13 V among the synthetic samples (2 and 5 wt % GO composites). A prolonged (3600 sec) constant current response shows rapid kinetics, whereas a lower Tafel slope and lowest resistance represent the material's stability.[65]

Li et al. (2018) demonstrated how to use the simplest electrochemical activation technique to produce a bimetallic (Pt-Ni) nanoparticle composite on a nickel framework surface. The EASA of Pt/p-Ni nanoparticles was around two times higher than that of Pt/C composite.[66]

Ortega and colleagues first proposed a simple impregnation approach in 2018 to create Pt-Ni/C

electrocatalyst. Characterization tests verified the presence of both metals, reduction in size of platinum nanoparticles because of nickel integration, and large surface area. Additionally, charge transfer process is accelerated by the reformed electronic structure caused by the synergetic action of two metals, the growth of metal oxides, and the minimization of CO adsorption during the oxidation process. [67]

In 2018, Chen et al. promised that $CuO/Co(OH)_2$ hybrid nanosheets with a well-balanced Co/Cu ratio will be used for MOR in an alkaline medium. Because of its high TOF, high surface area and insignificant Tafel slope, optimized copper content composite with high binding energy promotes cobalt oxidation and provides the highest current density[68]

In 2018, Askari and coworkers developed a trimetallic sulfide/graphene hybrid by hydrothermal method. During Tafel slope analysis, the resulting electrode exhibits appropriate catalytic characteristics and a sizable diffusion current. A significant number of electroactive sites and graphene's conductivity have been demonstrated by electrochemical testing, and two metals (Ni and Co) have been shown to enhance the surface efficacy and permit a smooth electron transport process.[69].

In 2019, Noor et al. reported Cu-BTC MOF/GO composites via CV, CA, and Tafel slope in basic medium. They explored their electrocatalytic return in detail as well. The MOR has good performance for a 3D cuboid MOF. Of the developed samples with different GO concentrations ,Cu-BTC-5 wt% of GO composite achieved 120 mAcm^{-2} at 0.81V vs. Ag/AgCl .The material described above is a competitive alternative to expensive noble metal-centered electrocatalysts due to its low resistance, high diffusion co-efficient, and long-range stability (3600 sec).[70]

In 2019, Bu et al. synthesized and in-depth examined a new Nickel based material with a cubane cluster for oxidation reaction in the presence of methanol. 0.029 A/cm^2 current density is seen at 1.56 V in the tested sample with resistance (90) and durability for 2000 seconds. [71]

Chapter 3: Experimental Details

3.1 Materials used.

The list of chemicals and reagents along with sources and % purity is mentioned below. All chemicals and reagents were utilized without further purification treatment.

- Solvents: (DI water, 99 %, Merck)

 (ii) C_2H_5OH (Ethanol, 99 %, Merck)

(iii) CH_3OH (Methanol, 99 %, Merck)

- Metal salts:

- $Ni(OAc)_2.6H_2O$ is 98 %, Sigma Aldrich

- $Co(NO_3)_2.6H_2O$ is 98 %, Sigma Aldrich

- $Cu(NO_3)_2.3H_2O$ is 98 %, Sigma Aldrich

- Bases :

- (i) KOH is 98 %, Sigma Aldrich

   (ii) NaOH is 98 %, Sigma Aldrich

3.2 Synthetic Schemes

All the electrocatalysts synthesized for this thesis report are based on copper-based materials. Hydrothermal synthesis method is utilized for the fabrication of these catalysts.

3.2.1 Synthesis of Ni-Cu Binary Metal Oxide

Ni/Cu binary oxide was produced by hydrothermally mixing two mmol of $Ni(Ac)_2.4H_2O$ with one mmol of $Cu(NO_3)_2.3H_2O$.After adding 40 mL Deionized water and stirring for 15 minutes, a clear solution was produced. The mineralizer 13 mmol urea was then added to control the crystal shape

and structure. The Teflon line autoclave was then filled with this solution and kept in the heating oven for 12 hours at 160 degrees. After being centrifuged twice with deionized water and ethanol at 8000 revolution per minute for 10 minutes each, the resultant solution was dried for a whole night in a vacuum oven at 60 degrees. After being calcined at 450 $^\circ$ C for four hours, the powder was created. Different nickel to copper ratios (2:1, 1.5:1.5, 1:2, 2.5:0.5, and 0.5:2.5) were used to generate a series of Ni-Cu-O samples, which were then designated as HN1, HN2, HN3, HN4, and HN5, accordingly. (Figure 3)
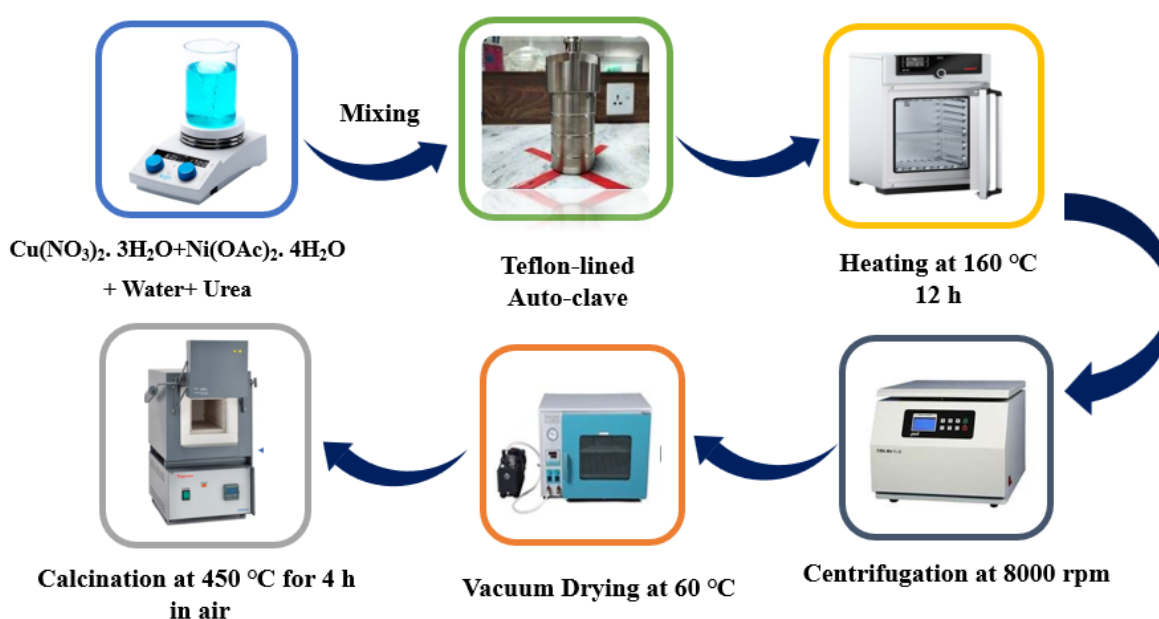
Figure 3: Hydrothermal Synthetic scheme of the Ni/Cu binary metal oxide

3.2.2 Synthesis of Cu/Co Binary and ternary metal composites

3.2.2.1 Binary Metal oxide preparation:

Typically, 40 mL of DI water were combined with two milli moles of $Cu(NO_3)_2.3H_2O$ with one milli mole of $Co(Ac)_2.4H_2O$. It received 18 mmol NaOH and was stirred for 15 minutes at room temperature before being placed to a 75 mL Teflon lined autoclave .Next, a heating oven at 373 K was used to heat

the Teflon autoclave for 10 hours. The resultant solution was then dried for six hours at 373 K in a vacuum oven after being centrifuged twice with deionized water and ethanol at 8000 revolution per minute for 10 minutes each. The obtained powder was calcined for six hours in air at 673K. Different copper to cobalt ratios (1:2, 1.5:1.5, 2:1, 2.5:0.5, and 0.5:2.5) were used to generate a series of Cu-Co-O samples, which were then designated as HC1, HC2, HC3, HC4, and HC5, accordingly. A schematic description of the whole process is shown below.
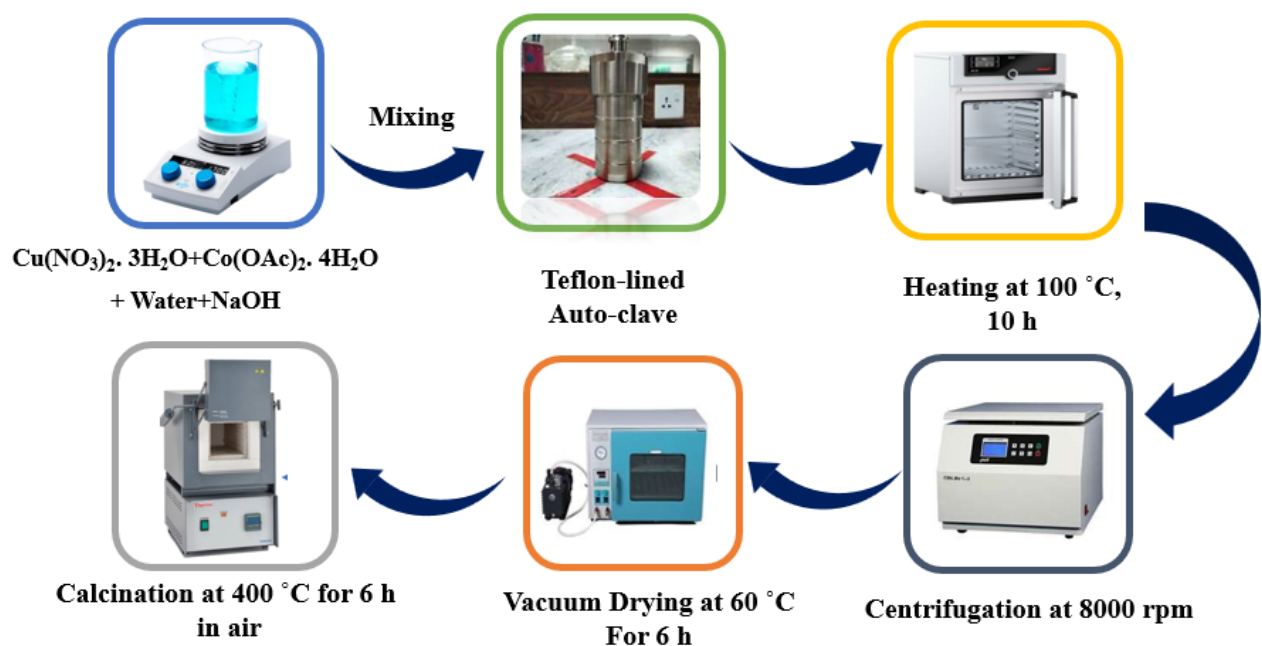
Figure 3.1 : Hydrothermal Cu/Co binary oxide synthesis

3.2.2.2 Ternary metal oxide preparation:

Various moles of Ni were employed to hydrothermally synthesize the ternary metal composite using the optimal binary oxide ratio. 2.5 milli moles of Cu (NO_3) $_2$. $3H_2O$ with 0.5 milli moles of Co $(Ac)_2$.$4H_2O$ and 0.25 milli moles of Ni (Ac) $_2$.4 H_2O were mixed in 60 mL of deionized water. Then 18 milli moles of NaOH were added and resultant mixture was swirled to create a homogeneous mixture. The Teflon lined autoclave was then used to heat this solution in heating oven for 10 hours at 373K. The resulting solution was then centrifuged twice with Deionized water and ethanol at 8000 rpm for 10

minutes each before being dried for six hours at 373 K in a vacuum oven . The dried sample was then kept in muffle furnace at 400 ° C for six hours in air for calcination and obtained power was grinded to obtain powdered form of the product. Three different ratios of the ternary composite are prepared by using HC4 binary metal oxide ratio with 0.25, 0.5 and 1mmol of $Ni(OAc)_2.4H_2O$,represented by HCNi8, HCNi9 and HCNi10. The schematic diagram is depicted below in Figure 3.2
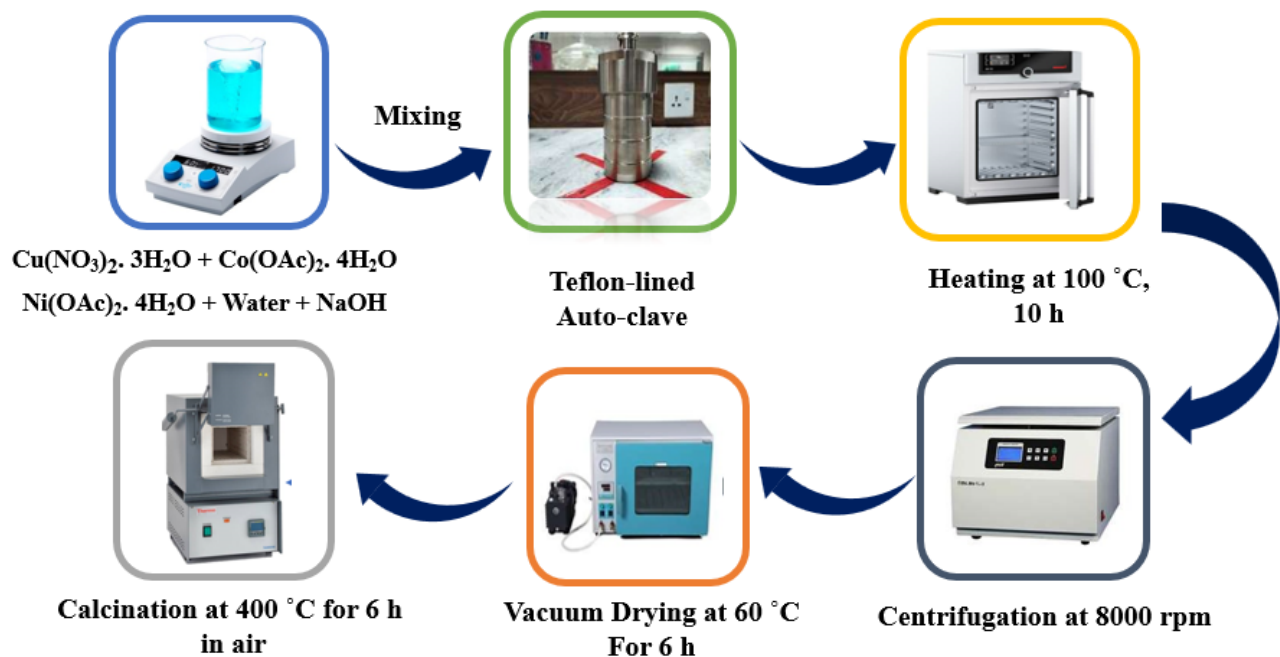

Figure 3.2 : Cu/Co/Ni ternary metal composite synthesis

3.2.2.3 Electrode preparation:

The electrodes were made of Ni-foam. The nickel foam with dimension 1.5 cm^2 *1 cm^2 was first cleaned with a 1 M HCl solution, followed by 15 minutes of sonication with ethanol and deionized water, and overnight drying in a vacuum oven. Then the obtained slurry was deposited by sonication for two hours using 2 mg of the active component, 10 uL of a nafion-based binder, and 100 uL of ethanol in an Eppendorf. This slurry was applied on clean Ni-foam using a micropipette, and it was then given the night to dry in a vacuum oven.
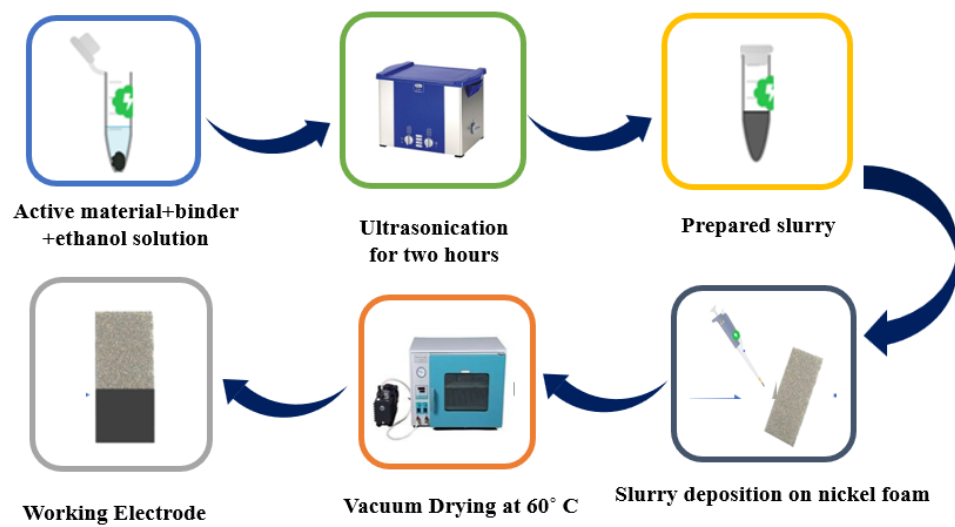
Figure 3.3 : Electrode preparation steps

Chapter 4: Results and Discussion

4.1 Ni/Cu Binary Metal Oxides

Ni/Cu binary metal oxides have been synthesized by hydrothermal method to have a controlled morphology and crystal size to use them as an effective water and methanol oxidation electrocatalyst.

4.1.1 X-ray Diffraction analysis of Cu-Ni bimetallic oxide

The crystal structure and phase composition of the prepared samples were assessed by X-ray Diffraction analysis. The dominating composition of CuO in the composite samples is shown by the patterns' significant diffraction peaks, which are monoclinic CuO crystals (JCPDS No. 01-002-1040), as shown in Figure 4. In relation to the (1 1 1), (200) and (220), (311) and (222) planes, three faint diffraction peaks of cubic NiO (JCPDS No. 01-002-1216) can be detected at 37.28, 43.25,62.72,75.37, and 79.87°. NiO peak intensities steadily rose as Nickel precursor concentration in the ratios increased, but CuO peak intensities declined. The XRD results support the materials' nickel oxide and Copper oxide crystallization.
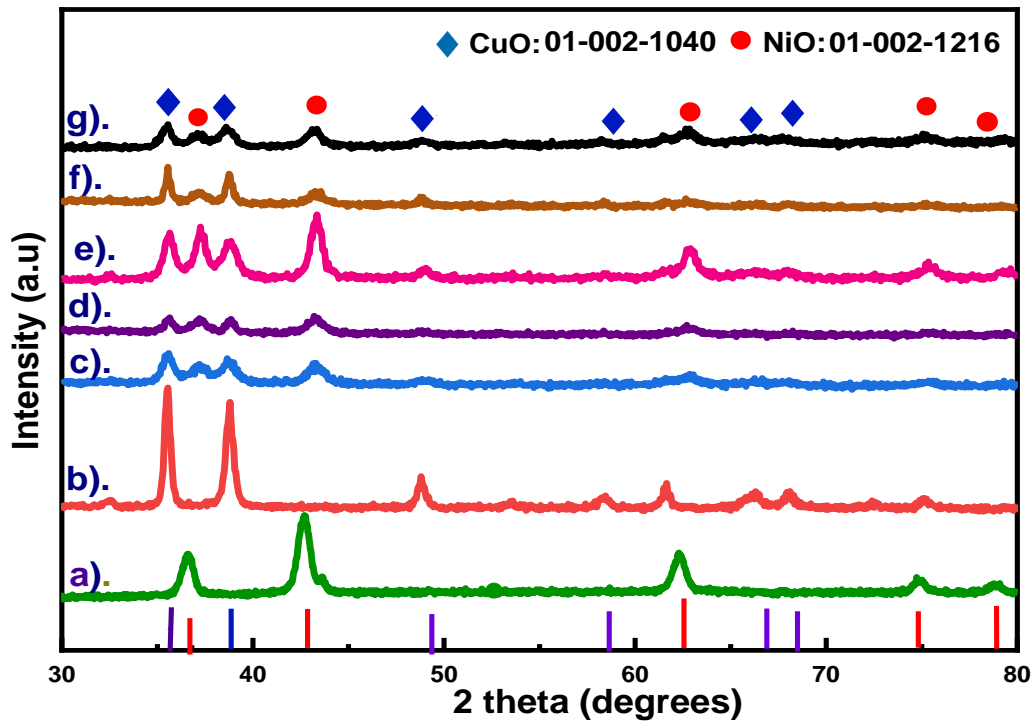
Figure 4: XRD patterns of a) NiO (b) CuO (c),(d),(e),(f) and (g) are Ni/Cu Ratios
NC1,NC2,NC3,NC4,NC5

4.1.2 Scanning Electron Microscopic analysis of Ni/Cu oxides

The Copper oxide nanoparticles showed a quasi-spherical shaped morphology, according to the SEM pictures. The hydrothermal method produced small quasi-spherical particles of homogeneous dimension (Figure 5a). While Nickel oxide particles revealed rod shaped morphology and they were present in the form of brain like aggregates with an average size of 78 nm. The SEM analysis of Ni/Cu binary oxide exhibits both morphologies of CuO and NiO showing uniform particles distribution. EDX analysis further confirmed composition of the samples according to which Ni/Cu binary oxide contains nickel, copper, and oxygen atoms while EDX of individual metal oxides confirmed presence of copper and nickel and oxygen, confirming the synthesis of pure metal oxides with no impurities. (Figure 5a,b,c)
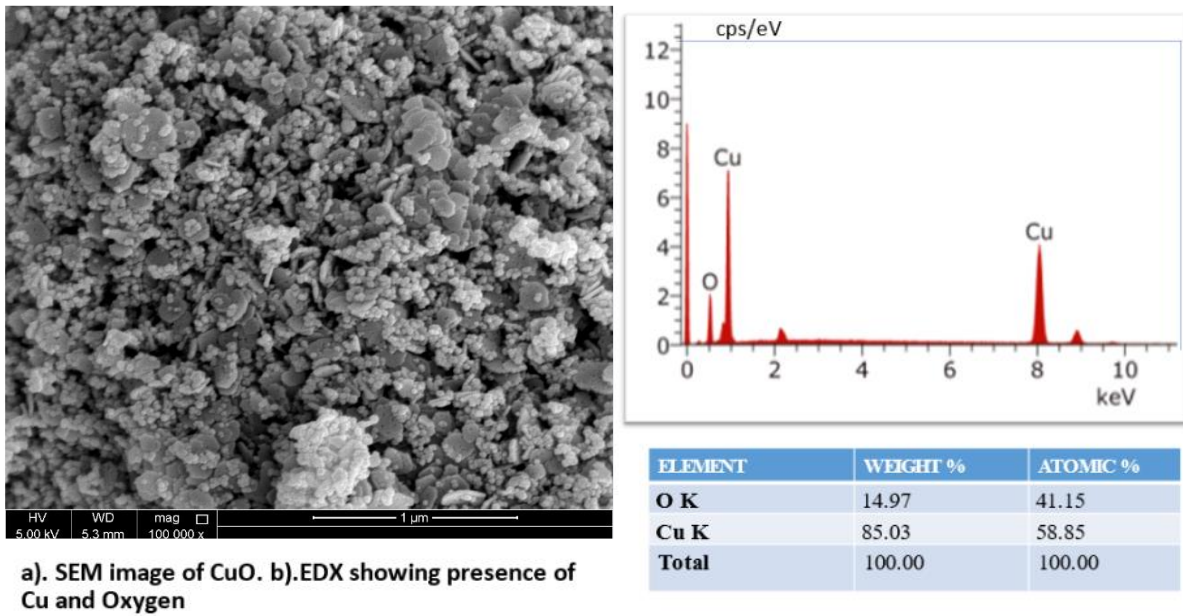
ELEMENT	WEIGHT %	ATOMIC %
O K	14.97	41.15
Cu K	85.03	58.85
Total	100.00	100.00

a). SEM image of CuO. b).EDX showing presence of Cu and Oxygen

Figure 5a: SEM / EDX Analysis of Copper oxide

ELEMENT	WEIGHT %	ATOMIC %
O K	14.88	39.08
Ni K	85.12	60.92
Total	100.00	100.00

a). SEM image of NiO. b).EDX showing presence of Ni and Oxygen
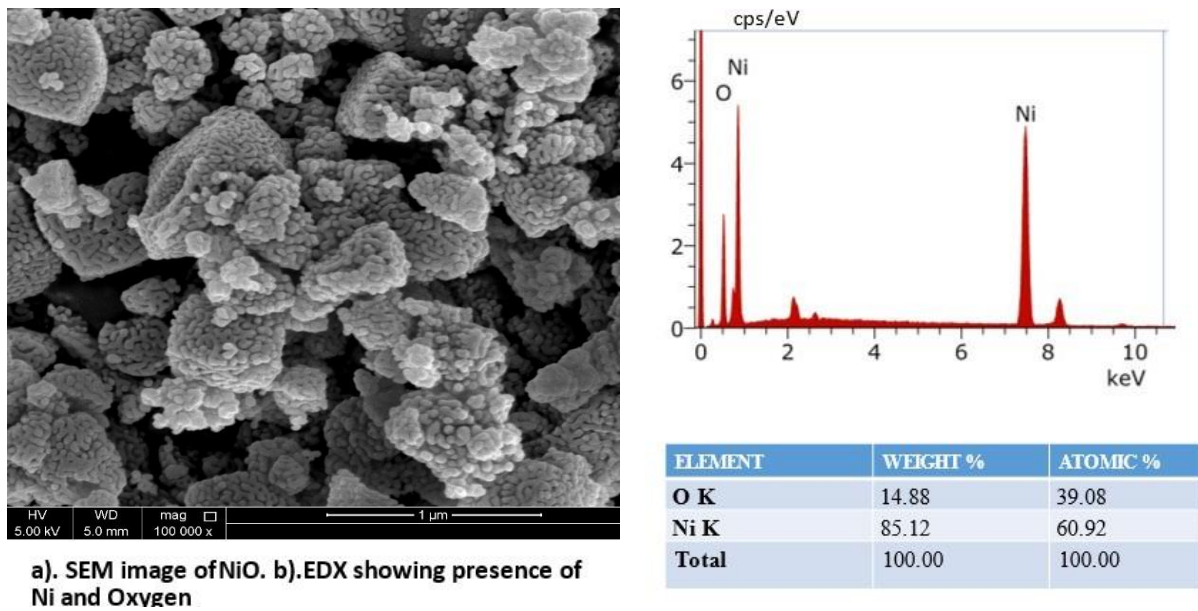
Figure 5b: SEM / EDX Analysis of Nickel oxide

32

ELEMENT	WEIGHT %	ATOMIC %
O K	15.29	41.27
Ni K	20.45	15.05
Cu K	64.26	43.68
Total	100.00	100.00
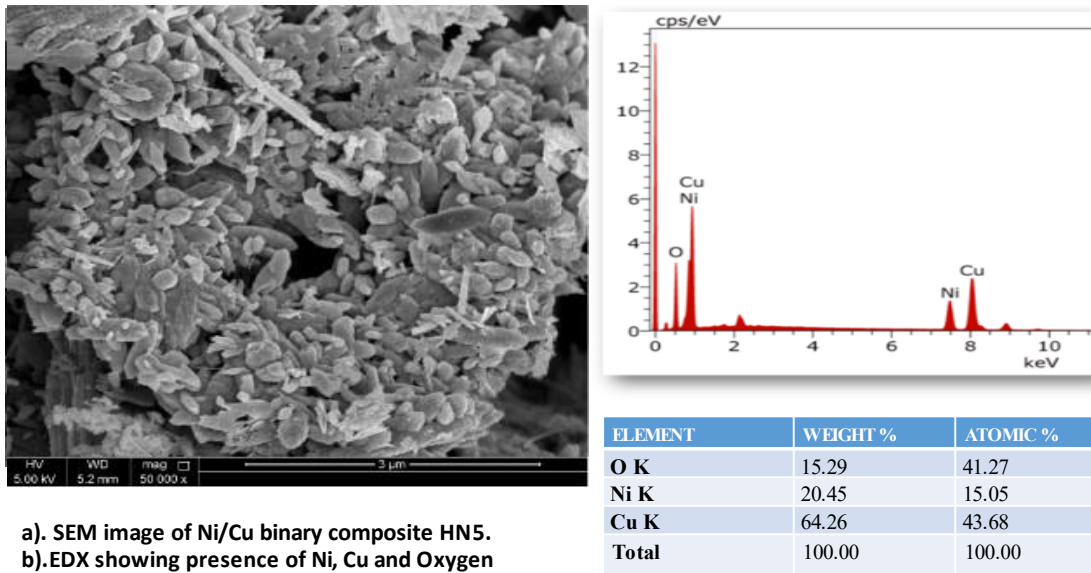
a). SEM image of Ni/Cu binary composite HN5.
b).EDX showing presence of Ni, Cu and Oxygen

Figure 5c: SEM / EDX Analysis of Copper oxide/Nickel oxide binary composite

4.1.3 Transmission Electron Microscopic analysis of Ni/Cu oxides

Morphology of the nickel oxide and nickel copper binary oxide was further investigated by TEM analysis. Figures 6(a,b,c) reveal quasi shaped CuO (crystallite size :33 nm), rod shaped NiO (crystallite size :78 nm) and highly porous morphology of Ni/Cu oxide having lighter and darker areas [72] and have crystallite size range of 90-133 nm.
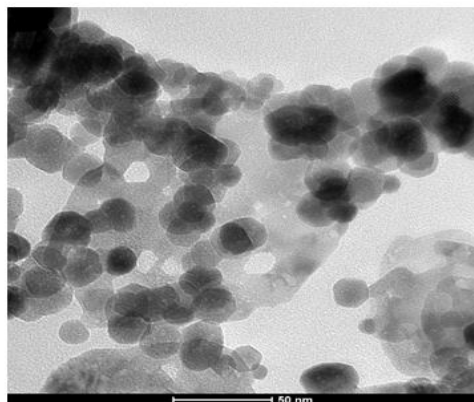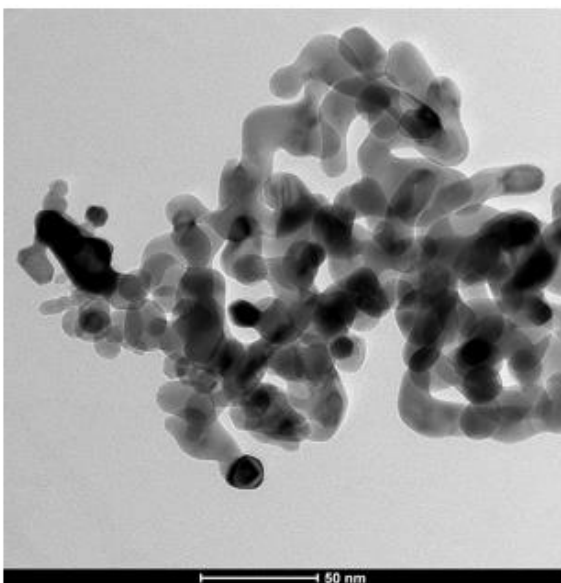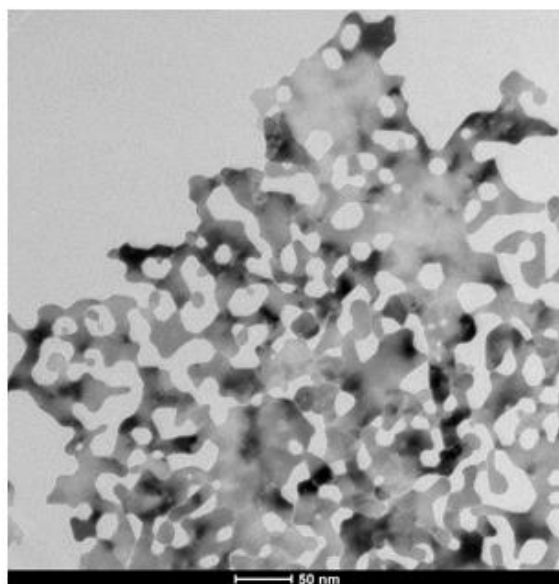
Figure 6a TEM analysis of CuO

b)TEM image of NiO Particles

c)TEM image of Ni/Cu composite

Figure 6 (a, b and c): TEM Analysis of Ni/Cu binary composite and Nickel oxide

4.1.4 Electrochemical Studies of Ni/Cu Binary metal oxides

4.1.4.1 Water Oxidation reaction

Electrochemical measurements of the electrodes were done by using potentiostat and its response was recorded in the form of LSV curves. The water oxidation electrocatalytic activity of the binary metal

oxides is appreciably higher than individual pure oxide which confirm that synergistic effect between nickel and copper both metals resulted in the turning of their electronic structures in such a way that their catalytic activity was enhanced because the solution's charge transfer resistance has decreased. As a result of this, more active sites are available and depending upon the relative ratio of both oxides, the electrode-electrolyte interface development occurs in diverse ways that leads to high OER activity. Ratio HC-4 being the optimized binary ratio shows maximum OER activity. A trend among the OER activities of the ratios was developed which demonstrates that by increasing the amount of copper and by decreasing the amount of cobalt in the binary composites, OER activity increases. This trend is further confirmed by EIS which showed that the highest OER active catalyst has smallest C_{dl} resistance. Tafel plots are another authentication of the catalyst activity. The ideal catalyst possesses the low value of Tafel slope to allow for enhanced current at low overpotentials. Because of their powerful synergistic catalytic effect, the optimized Ni-Cu bimetallic oxide HN5 surpassed monometallic oxides in terms of bifunctional catalysis. As it is evident from the figure that the electrocatalyst showing the best OER activity has smallest Tafel slope and hence faster charge transfer kinetics. (Figure 7 and 8)
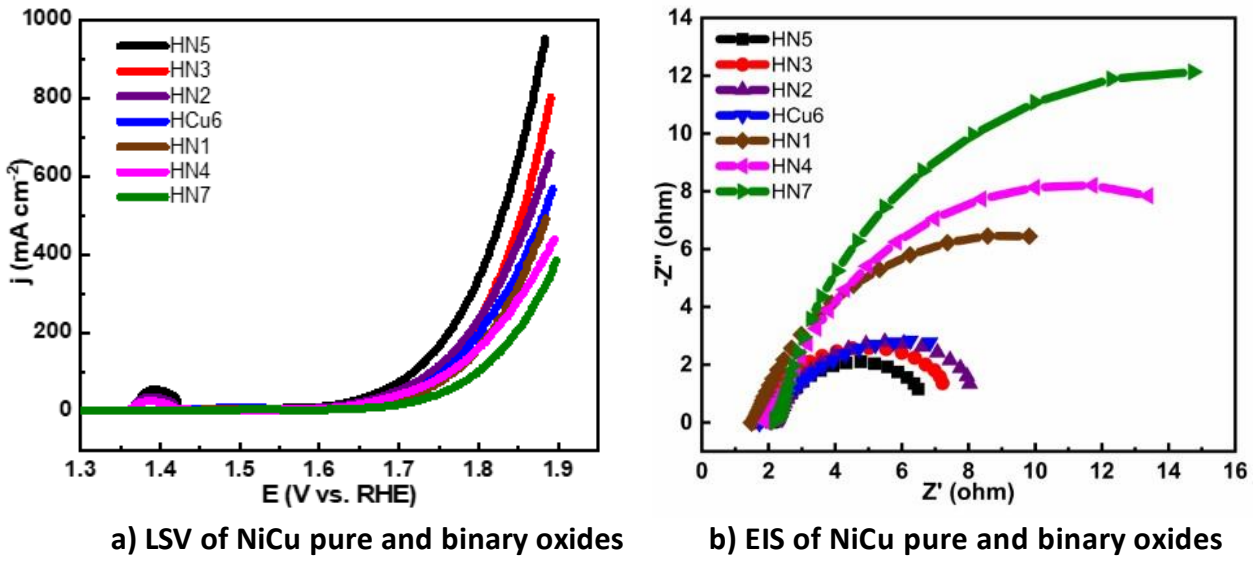
a) LSV of NiCu pure and binary oxides

b) EIS of NiCu pure and binary oxides

Figure 7: LSV curves and EIS analysis of pure and binary Ni/Cu oxide

c) Tafel Plots of NiCu pure and binary oxides

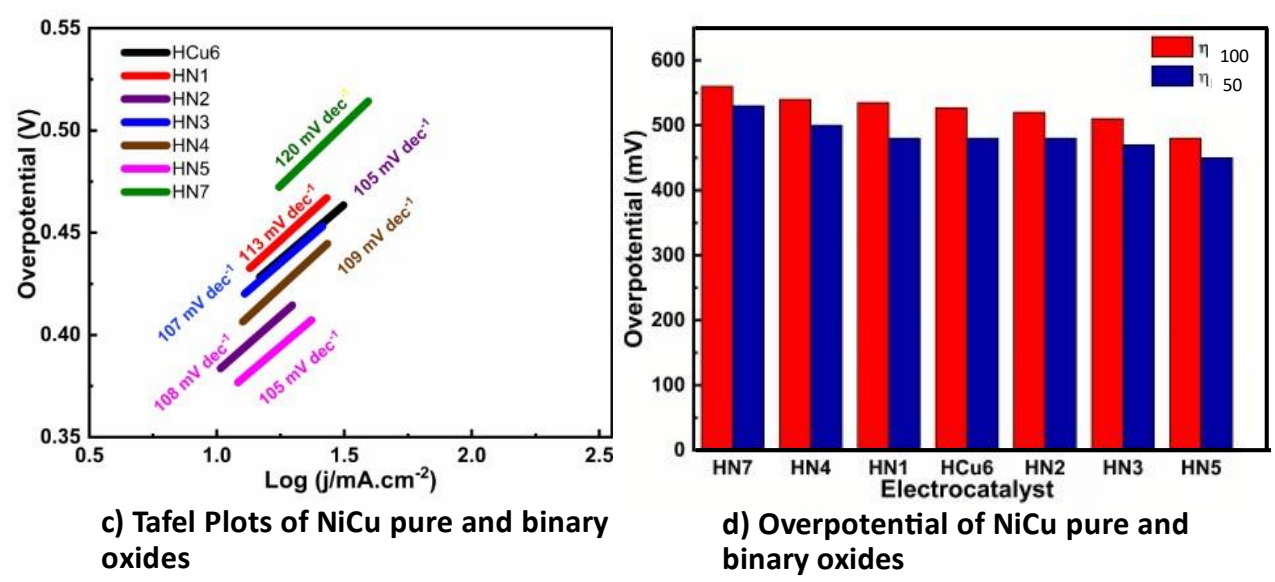**d) Overpotential of NiCu pure and binary oxides**

Figure 8: Tafel plots and overpotential of pure and binary oxides

4.1.4.2 Methanol Oxidation

Firstly, pure oxide with binary oxides and then all binary oxides were tested for methanol oxidation activity as well. LSV curves showed positive response for MOR activity suggesting the suitability of the binary catalysts for oxidation of methanol. It is evident from the graphs that by increasing the concentration of methanol in the solution, MOR activity increases until it reaches a saturation point of 0.4 mL. (Figure 9-14)

The onset potential is one of the key indicators used to show electrocatalytic activity. In general, alcohol electrooxidation systems with higher negative start potential exhibit more catalytic activity and less over potential. The measured onset potential of the binary oxides, as shown in Figure 9, is 0.33 mV (vs. Ag/AgCl). Furthermore, it is evident from the graphs that the onset potential is solely dependent on the binary oxide composition and is unaffected by the methanol concentration. The optimal ratio for the MOR activity is NC5, which has the maximum current density of 694 mAcm^{-2} and an onset potential of 0.3 V.

Overall, the results show that the creation of ZOOH/Z(OH)$_2$ on the surface of Z catalyst—whose optimal composition is Cu 2.5 mL and Ni 0.5mL is accountable for the distinct electrocatalytic activity of the best ratio. The following reactions help to explain how ZOOH layers develop for giving MOR activity.

Due to the electron arrangement of the Z binary composite particles, which facilitates the creation of a stable hydroxide layer, synthesis of Z(OH)$_2$ was done on their surface.

$$Z(OH)_2 + OH^- \rightleftarrows ZOOH + H_2O + e$$
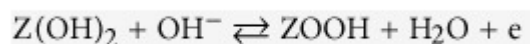
With increasing potential sweeps, the current density values gradually rise due to OH entering the Z(OH)$_2$ surface layer. High catalytic activity is produced because of the increasing creation of a thick ZOOH layer which is analogous to the transition of Z(OH)$_2$/ZOOH. This means that the method for

electrooxidizing methanol using the recently developed NiCu binary composite is compatible with prior literature. The created catalyst (Z) adsorbs the methanol in the first stage of the methanol oxidation and releases some protons; however, more protons are released in the second and third stages. The Z_3COH species typically disintegrates in step 4, producing Z and protons.[73]

The oxidation of methanol was also studied by utilizing electrochemical impedance spectroscopic technique. The Nyquist plots from EIS data for the tested electrodes at different concentrations of methanol are displayed in Figure (9-14). The resultant figure, which takes into consideration the electrode's Nyquist plot, shows that the current causes the double layers to capacitively charge and with the increase in the concentration of methanol, the diameter of semicircle decreases accordingly. So, the highly efficient ratio has the lowest diameter.

In addition to achieving the required high electrocatalytic performance, the composite structure's stability was a goal. The chronoamperogram of an electrode was recorded in for about 25 h s at a fixed potential (E = 0.1 V) as shown in Figure 15. The graph displays an early reduction in current followed by a somewhat steady decline. It is important to highlight that just five binary composite ratios were functional electrodes for the duration of the electrochemical study. Numerous electrode applications had no effect on the performance, demonstrating the catalyst's outstanding stability. Figure 15 supports the hypothesis that the composite structure contributes to the extraordinary stability of the implanted catalyst.
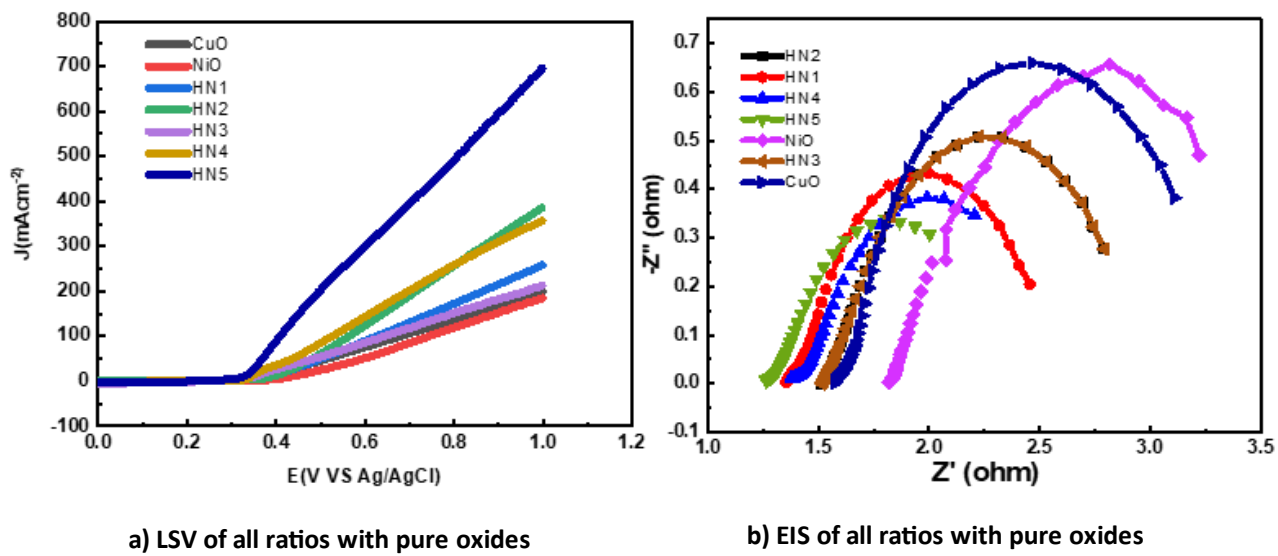
a) LSV of all ratios with pure oxides

b) EIS of all ratios with pure oxides

Figure 9: LSV Curves and EIS analysis of all ratios and pure oxides for methanol oxidation

a).LSV of HN1

b).EIS of HN1
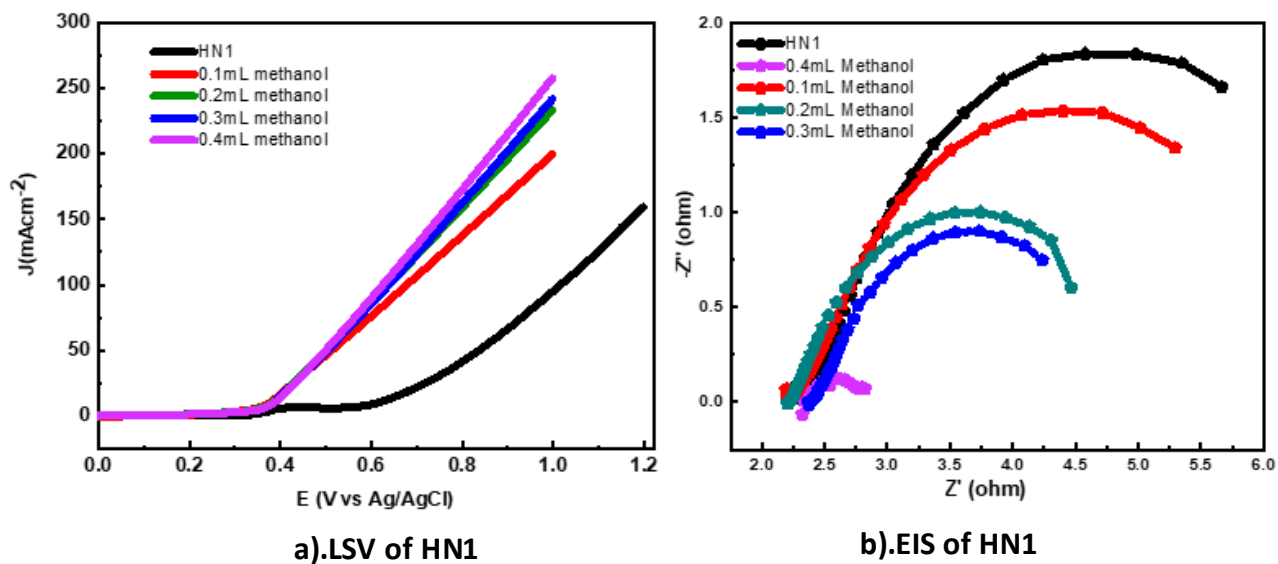
Figure 10: LSV and EIS curves of HN1

a).LSV of HN2

a).EIS of HN2
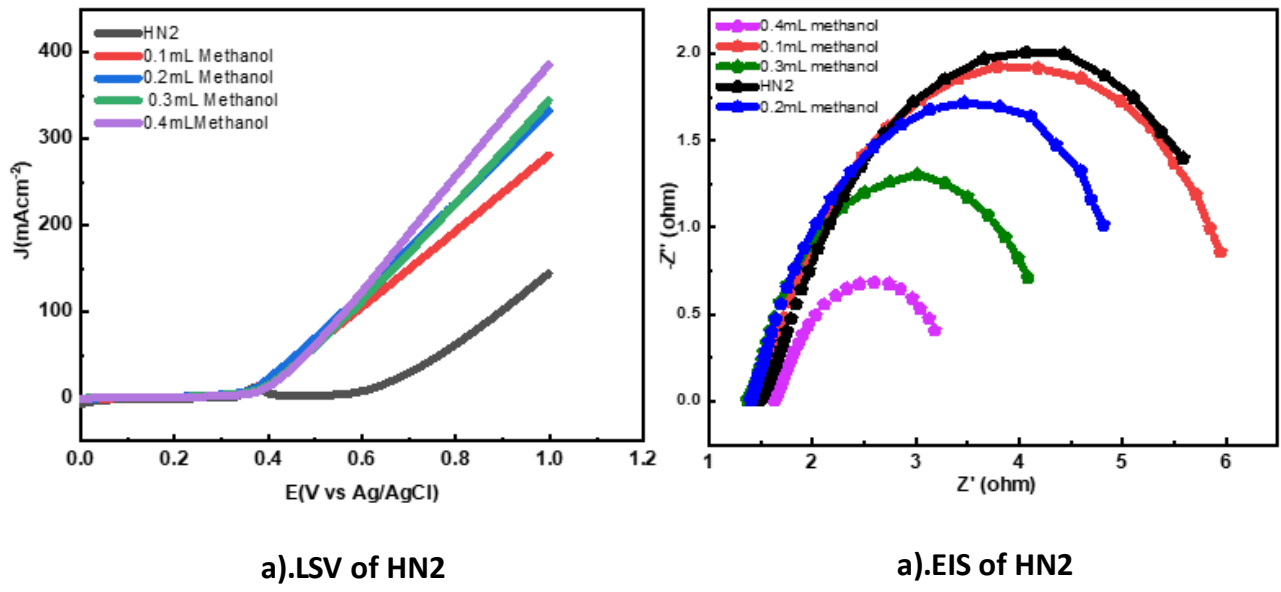
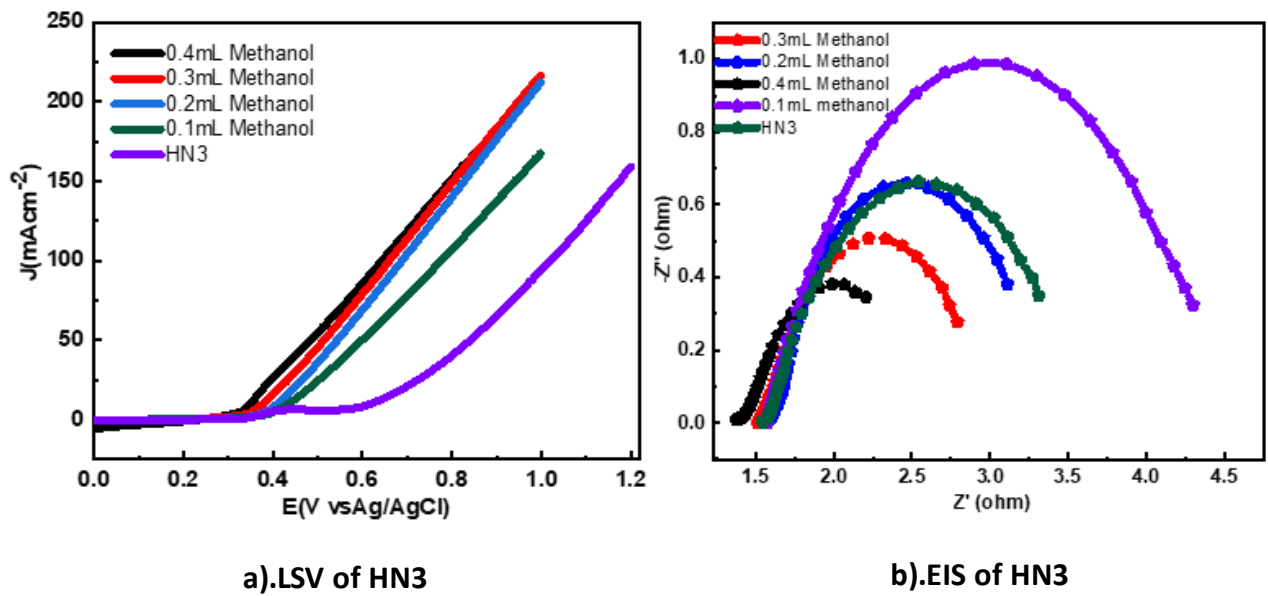Figure 11: LSV and EIS curves of HN2

a).LSV of HN3

b).EIS of HN3

Figure 12: LSV and EIS curves of HN3

a).LSV of HN4

b).EIS of HN4

Figure 13: LSV and EIS curves of HN4

a).LSV of HN5
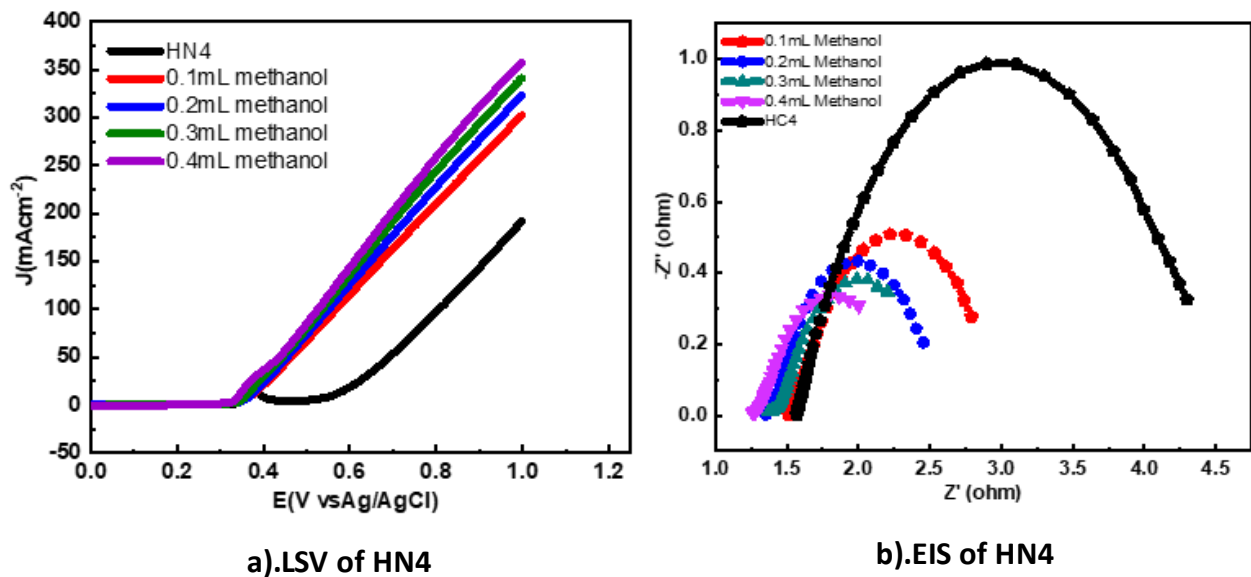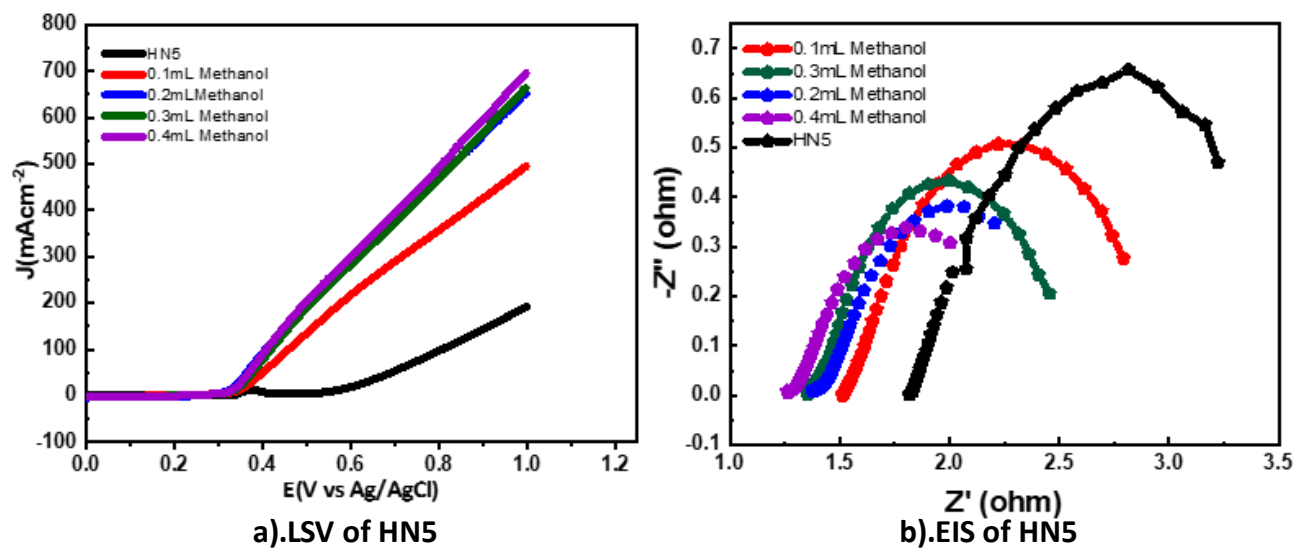
b).EIS of HN5
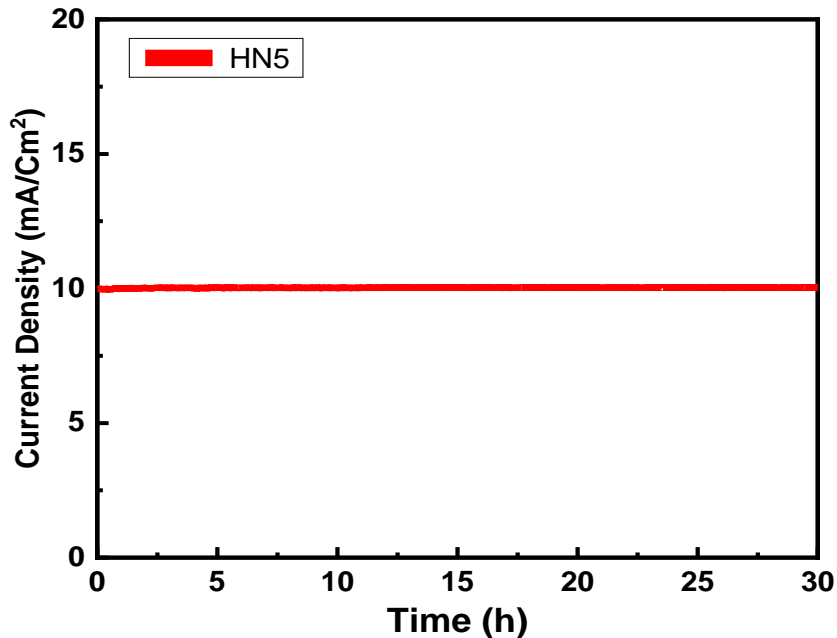
Figure 14: LSV and EIS curves of HN5

Figure 15: Chronoamperometry of HN5

4.2 Results and Discussion for Cu/Co Binary and Cu/Co/Ni Ternary Composites

Cu/Co binary and Cu/Co/Ni ternary metal composites have been synthesized through hydrothermal methods and are characterized to check their physical properties.

4.2.1 X-ray Diffraction Analysis:

The XRD pattern for all catalyst ratios revealed common diffraction peaks at 31.2°, 36.9°, 56.1°, and 59.5° that were attributed to (220), (311), (422), and (511) planes, respectively, and were well-matched with $CuCo_2O_4$ (JCPDS # 00-001-1155), while the peak at 35.5°, 39.1°, 48.6°, 54.05°, 61.7°, 66º are peaks of CuO.(Figure 16) The Ni oxide is supported by peak 43.0° (002) out of all the observed peaks. (Figure 17). By gradually increasing the quantity of copper and nickel in the cobalt lattice, a combination metallic structure is created that dramatically increases electron transport efficiency and encourages the kinetics of OER by improving material conductivity, and adds more active sites for
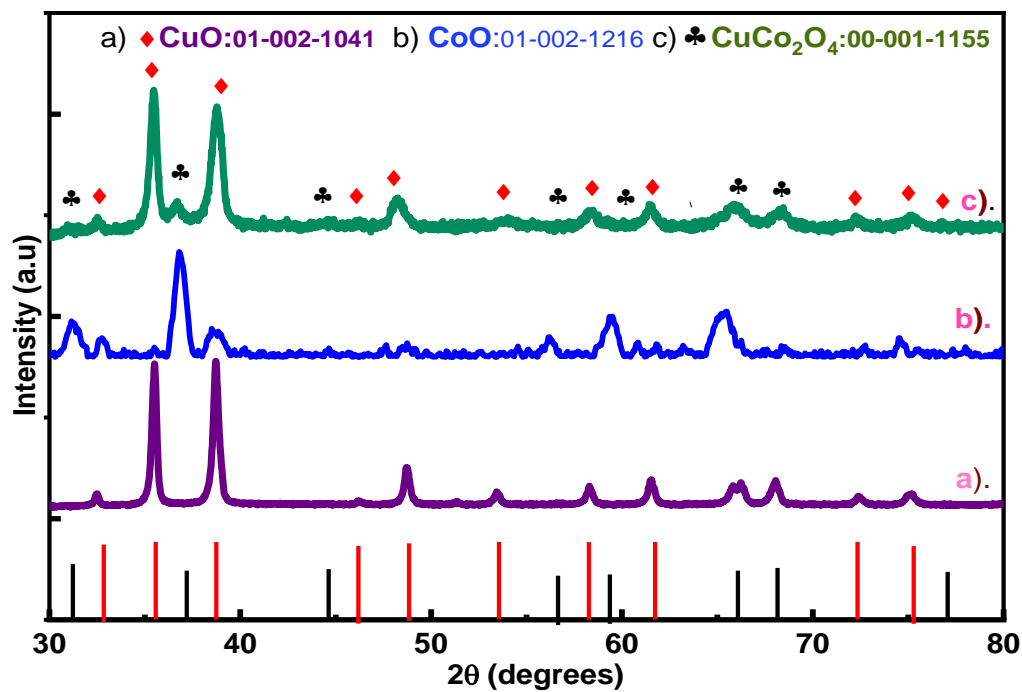
42

water splitting in general.[74],[75],[76, 77]

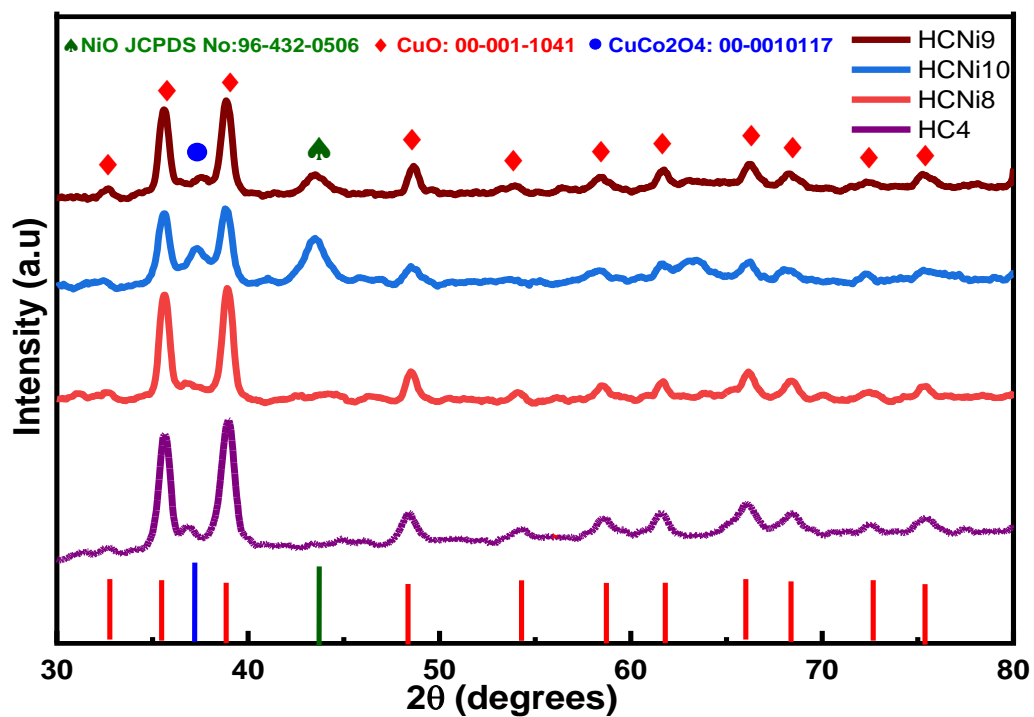Figure 16: XRD of a) CuO b)CoO c) CuCo binary metal composite HC4.

4.2.2 FTIR Analysis

FTIR Analysis shows Vibrational bands of Cu-O 434,456 and 484cm-[1], Co-O at 566cm^{-1} and Ni-O at

492cm^{-2}. (Figure 18).
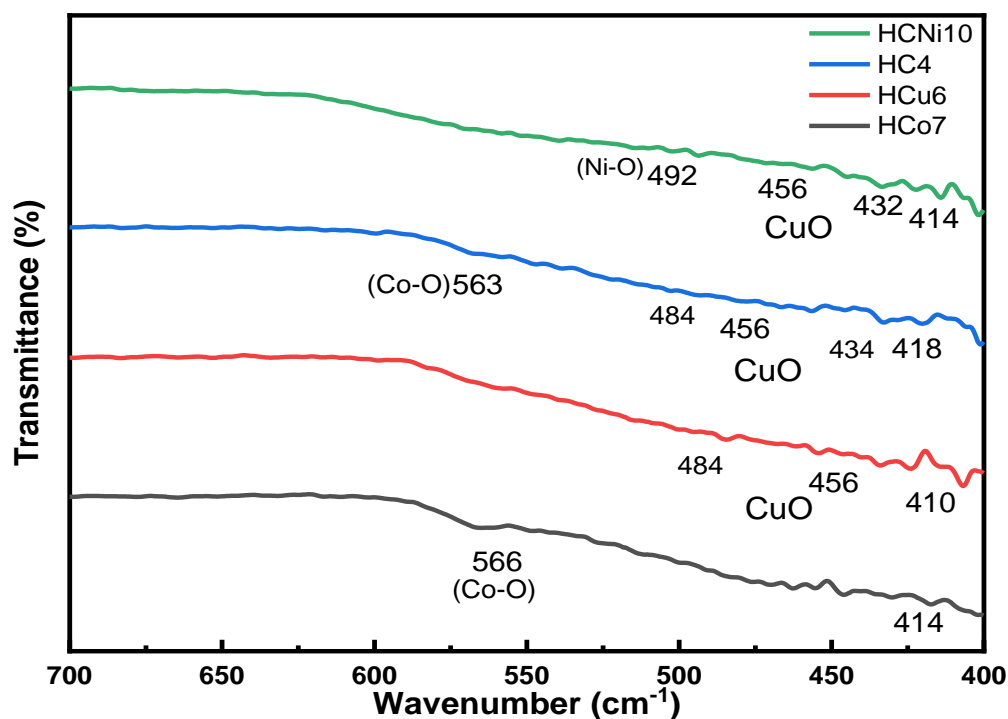
Figure 18 : FTIR of (a) CoO (b).CuO (c). Cu/Cu binary oxide and d) Cu/Co/Ni ternary metal

composites

4.2.3 Scanning Electron Microscopic Analysis

SEM analysis of cobalt oxide shows that it exhibits nanoflake like morphology that has an average

thickness of 0.662 micrometer (Figure 19). SEM analysis of Cu/Co binary oxide showed uniform

distribution of two types of morphologies ,having quasi spherical shaped morphology of copper oxide

and nanoflakes like structure of composite having small hexagonal spheres in it (Figure 20).

Compositional analysis also confirmed the presence of copper and cobalt along oxygen in powdered

sample. While the SEM analysis of ternary composite showed uniform distribution of three different types of morphologies thus confirming presence of nickel oxide particles in the form of spheres in the composite along copper and cobalt oxide composite .This evidence is further confirmed by EDX analysis which showed presence of nickel, cobalt and copper elements in the sample. (Figure 21)
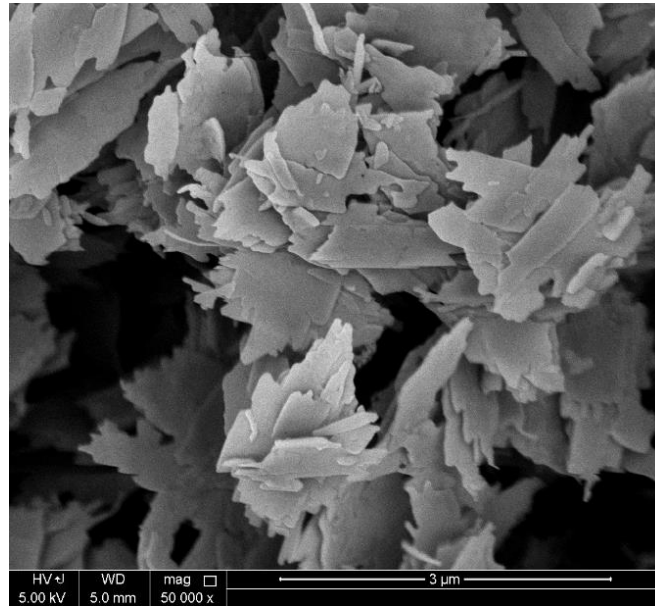
Figure 19: SEM analysis of Cobalt oxide

a). SEM image of CuCo binary composite H@.
b).EDX showing presence of Cu , Co and Oxygen
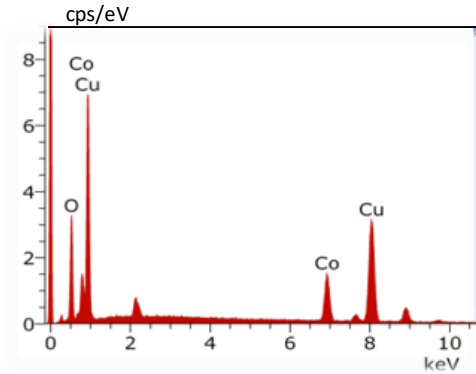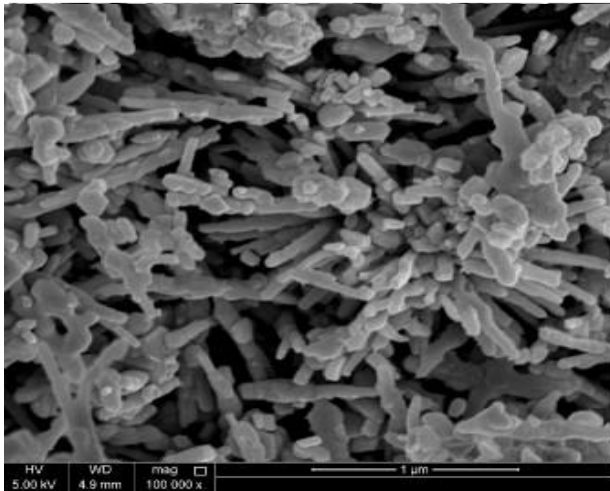
ELEMENT	WEIGHT %	ATOMIC %
O K	16.46	43.54
Co K	15.77	11.32
Cu K	67.77	45.14
Total	100.00	100.00

Figure 20: SEM analysis of CuCo Binary composite

a). SEM image of CuCoNi ternary composite HCNi10.
b).EDX showing presence of Cu , Co,Ni and Oxygen
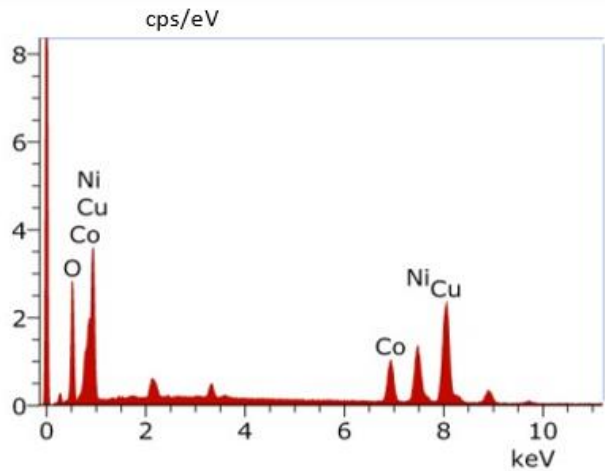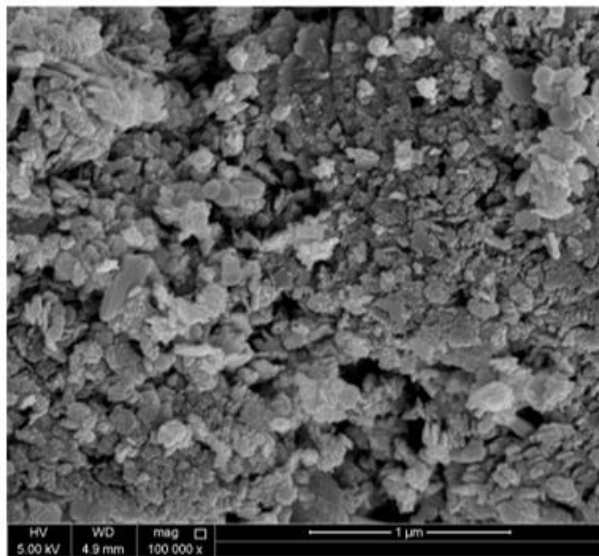
ELEMENT	WEIGHT %	ATOMIC %
O K	16.46	43.54
Co K	12.65	10.20
Cu K	55.05	39.71
Ni K	23.68	19.16
Total	100.00	100.00

Figure 21: SEM analysis of CuCoNi Ternary composite

4.2.4 Transmission Electron Microscopic Analysis

The morphology of the cobalt and copper binary and ternary oxide was further investigated by TEM analysis. Cobalt oxide nanoflake thickness is comparable with the SEM analysis thickness i.e., 660 nm. (Figure 22) While the binary and ternary composite also confirms the presence of two and three various types of morphologies and possess crystallite sizes in the range of 140-330 nm and 180-270 nm confirmed by SEM and EDX analysis (Figure 23).
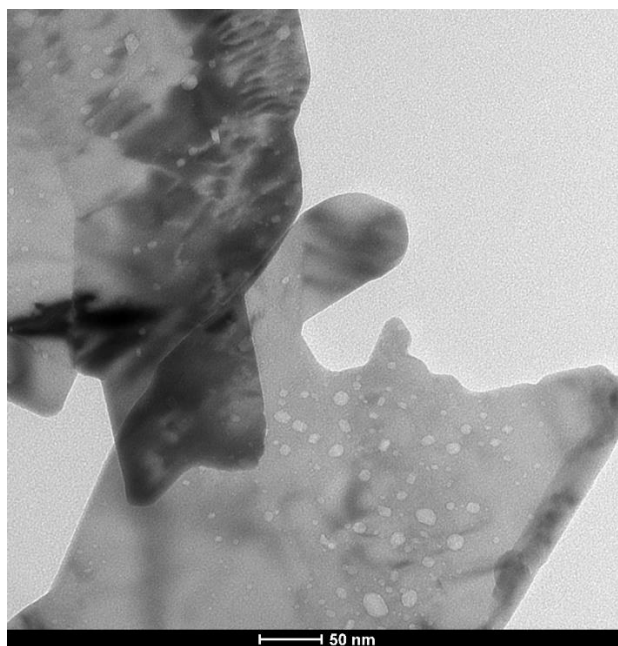
Figure 22 :TEM image of Cobalt oxide

a)TEM image of CuCo binary composite HC4 **b)TEM image of Cu/Co/Ni ternary composite HCNi10**
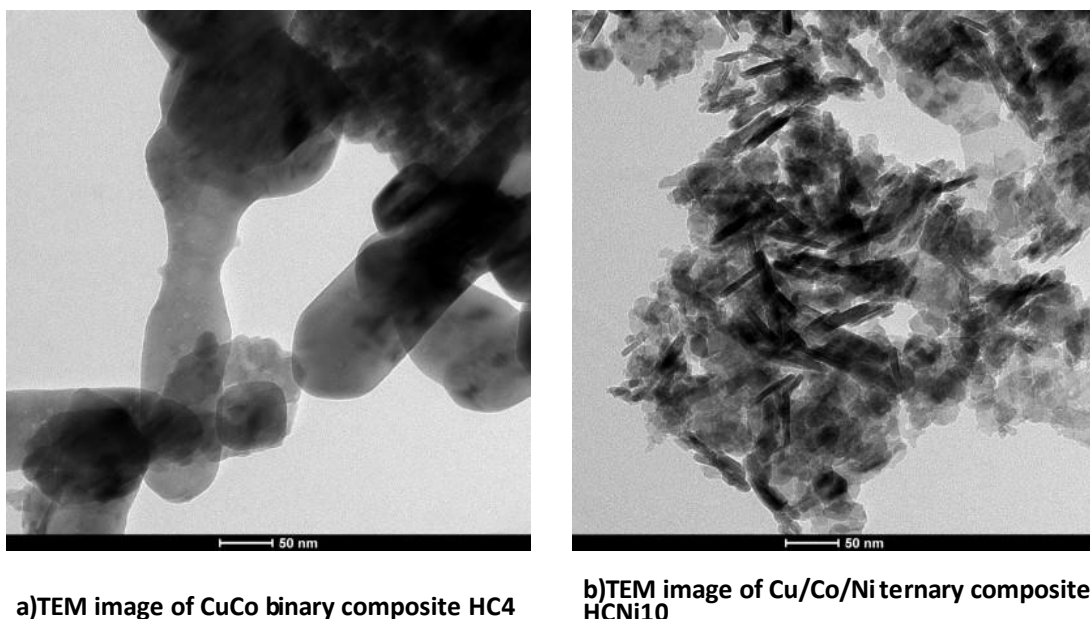
Figure 23 :TEM image of Cu/Co binary and Cu/Co/Ni ternary metal composite

4.2.5 Electrochemical Studies of CuCo binary and CuCoNi ternary metal composites

Electrochemical studies of the CuCo binary and ternary metal composites have been done by using three electrodes system in which platinum acts as counter electrode while Ag/AgCl act as reference electrode and electrocatalyst behaves as working electrode in 1 M HCl solution.

4.2.5.1 Water Oxidation Activity

CuCo binary and ternary composites' oxygen evolution reaction (OER) activities were assessed utilizing an alkaline solution (1 mol KOH) and a standard three electrode setup. To employ nickel foam electrodes (NF) as working electrodes, the composite powders were mixed with binder and ethanol and placed onto the electrodes. For comparison, blank Co_3O_4 nanoparticles and blank CuO particles ,results were also provided. Figure 16 shows the linear sweep voltammetry curves for different

48

ratios of Cu/Co metal oxides. It can be shown that every composite sample exhibited lower onset overpotentials than blank copper oxide and several of them even performed better in terms of electrochemical activity than blank Co_3O_4 nanoparticles. (Figure 24)

The composite sample HC4 and HCNi10, with an optimized composition showed incredibly small overpotentials (439 and 490 mV) and (411 and 441 mV) for current densities of 50 mA/cm^{-2} and 100 mA/cm^{-2}. The composite sample HC4 in the current investigation, which has the highest Cu content, displays least overpotentials than other ratios due to the highly conductive nature of copper. The improved electrochemical properties of the CuCo composites are further enhanced by the addition of nickel precursor which caused synergistic effect in ternary composite and tuned the structure in such a way to expose more active sites for OER activity thus enhances reaction kinetics. Further as the reaction mechanism changes ,junction is created, and different morphologies exhibit different active surface areas and hence exhibit variable OER activity.

To examine their catalytic kinetics towards OER, Tafel graphs of the CuCo binary composite and CuCoNi ternary composite , blank copper oxide and blank cobalt oxide nanoparticles, are provided in Figure 25. The Tafel slops of blank CuO , Co_3O_4 are higher than that of binary and ternary composites. Since Co_3O_4 nanoparticles , CuO and NiO particles work well together, the minimum Tafel slop of HCNi10 implies that the catalyst has a quicker OER speed and faster reaction kinetics. The information from Fig. 25b electrochemical impedance spectroscopy (EIS) reveals HC4 in binary and HCNi10 in ternary composites has least diameter of Nyquist plot which means they have a significantly lower value of charge-transfer resistance for water oxidation, which is advantageous to the electrochemical reaction process.(Figure 25,26)

Chronoamperometry was used to test the electrocatalyst's stability at 10mAcm^{-2}. Over the course of 25 hours, the best electro catalyst HCNi10 demonstrated a noticeably increased improvement in current

stability. (Figure 27)
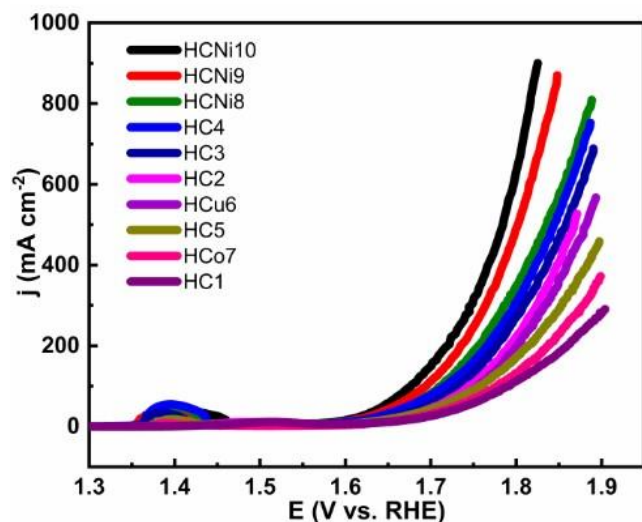
a) LSV of CuCo pure, binary and ternary composites
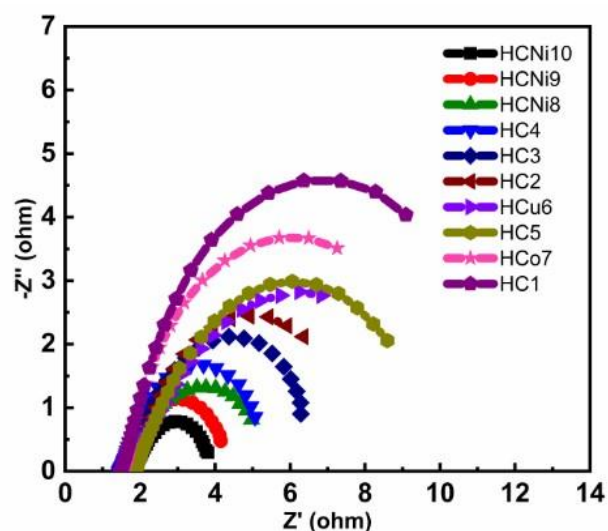
b) EIS of CuCo pure, binary and ternary composites

Figure 25. a and b : LSV and EIS curves of Pure Cu and Co oxides with binary and ternary oxides.
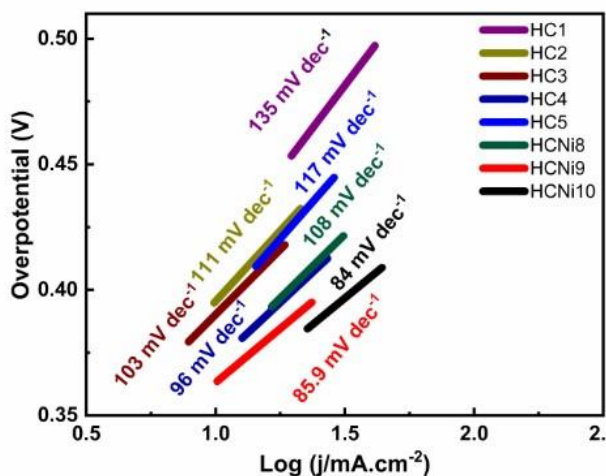
c) Tafel Plots of CuCo pure, binary and ternary composites
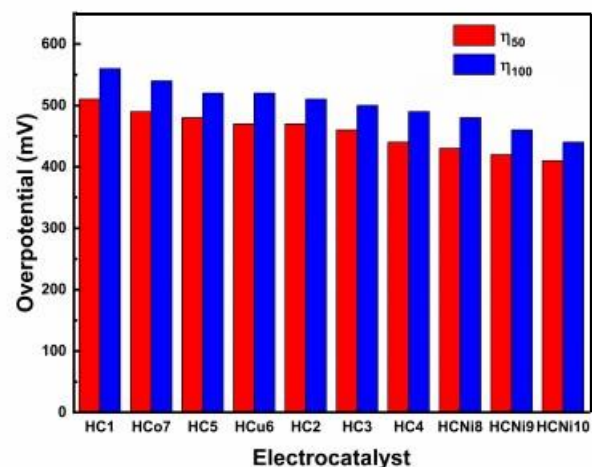
d) Overpotential of CuCo pure, binary and ternary composites

Figure 26. c) and d) : Tafel plot and overpotential profile of Pure Cu and Co oxides with binary
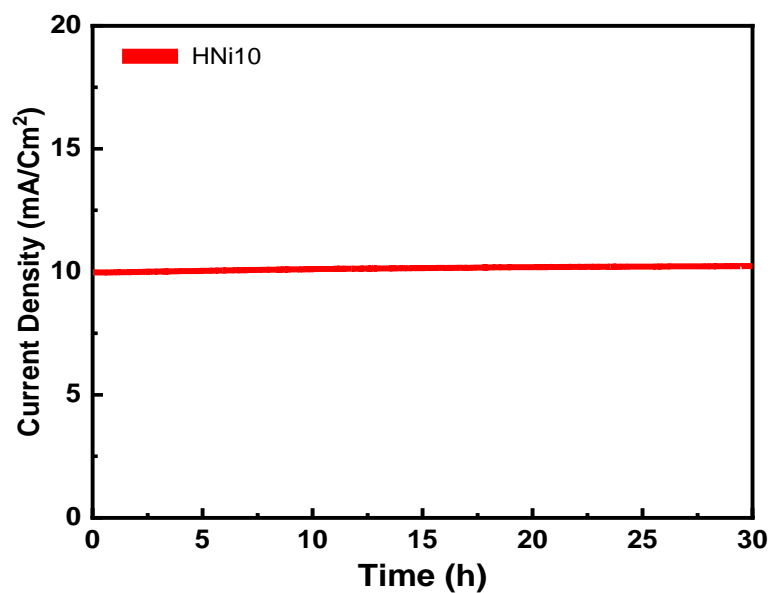
and ternary oxides.

Figure 27: Chronoamperometry for testing stability of electrocatalyst

Chapter 5   Conclusion

Modern characterization techniques confirmed the effective synthesis of the fundamental and composite materials. The electrocatalysis of the water and methanol oxidation process was found to be extremely efficient when employing the successfully synthesized nickel and copper oxide-based catalysts. The catalyst $Cu_{2.5}$ $Ni_{0.5}$ showed a 470 mV @ 50 mAcm^{-2} overpotential for oxidizing water while it showed excellent onset potential of 0.21 V at 0.4mL methanol oxidation Which is attributed to highly favorable network like structure. The porous morphology helped to expose more active sites for electrocatalytic processes and structure was synergistically tuned possessing uniform particle distribution. This favorable morphology reduced the solution resistance and led to faster OER and methanol oxidation kinetics.

 The catalyst $Cu_{2.5}$ $NiCo_{0.5}$ showed a 422 mV overpotential @ 50 mAcm^{-2} for oxidizing water.

The maximum j value that could be achieved for 0.4 V value was found to be 572 mA cm^{-2}.This outstanding OER performance of ternary metal composite is attributed to the strong electronic interactions between CuNi and Co metals which tuned the structure synergistically in a way that improved their OER kinetics by creating less solution resistance and more active sites ,thus speeding the overall reaction.

Chapter 5.1   Future Recommendations

✓ The hydrothermal synthesis technique can be used to create various OER and MOR catalysts.

✓ The activity of CuCo and NiCu can be further enhanced by incorporation of metal oxides, chalcogenides or CNTs.

✓ The synthesized materials can be used for photocatalytic water splitting.

✓ They can also be used as an electrode for a variety of batteries like Li-ion, Na-ion, K-ion batteries etc.

✓ They can also be used for energy storage applications ,e.g., supercapacitors.

References

1. *You, B. and Y. Sun, Innovative strategies for electrocatalytic water splitting. Accounts of chemical research, 2018. 51(7): p. 1571-1580.*

2. Wang, X., et al., *Metal–organic framework derived CoTe 2 encapsulated in nitrogen-doped carbon nanotube frameworks: a high-efficiency bifunctional electrocatalyst for overall water splitting.* Journal of Materials Chemistry A, 2018. **6**(8): p. 3684-3691.

3. You, B., et al., *Efficient H2 evolution coupled with oxidative refining of alcohols via a hierarchically porous nickel bifunctional electrocatalyst.* Acs Catalysis, 2017. **7**(7): p. 4564-4570.

4. Jiang, Y. and Y. Lu, *Designing transition-metal-boride-based electrocatalysts for applications in electrochemical water splitting.* Nanoscale, 2020. **12**(17): p. 9327-9351.

5. Saeedmanesh, A., M.A. Mac Kinnon, and J. Brouwer, *Hydrogen is essential for sustainability.* Current Opinion in Electrochemistry, 2018. **12**: p. 166-181.

6. Barber, J., *Hydrogen derived from water as a sustainable solar fuel: learning from biology.* Sustainable Energy & Fuels, 2018. **2**(5): p. 927-935.

7. Holladay, J.D., et al., *An overview of hydrogen production technologies.* Catalysis today, 2009. **139**(4): p. 244-260.

8. Safari, F. and I. Dincer, *A review and comparative evaluation of thermochemical water splitting cycles for hydrogen production.* Energy Conversion and Management, 2020. **205**: p. 112182.

9. Ahmad, H., et al., *Hydrogen from photo-catalytic water splitting process: A review.* Renewable and Sustainable Energy Reviews, 2015. **43**: p. 599-610.

10. Faber, M.S. and S. Jin, *Earth-abundant inorganic electrocatalysts and their nanostructures for energy conversion applications.* Energy & Environmental Science, 2014. **7**(11): p. 3519-3542.

11. Carrette, L., K.A. Friedrich, and U. Stimming, *Fuel cells: principles, types, fuels, and applications.*

ChemPhysChem, 2000. **1**(4): p. 162-193.

12.   Wang, Y., et al., *A review of polymer electrolyte membrane fuel cells: Technology, applications, and needs on fundamental research.* Applied energy, 2011. **88**(4): p. 981-1007.

13.   Matsuoka, K., Y. Sato, and K. Kawano, *Direct methanol fuel cell system.* 2004, Google Patents.

14.   Long, N.V., et al., *Novel Pt and Pd based core-shell catalysts with critical new issues of heat treatment, stability and durability for proton exchange membrane fuel cells and direct methanol fuel cells.* Heat Treatment-Conventional and Novel Applications, 1st ed.; Czwerwinski, F., Ed, 2012: p. 235-268.

15.   Vaghari, H., et al., *Recent advances in application of chitosan in fuel cells.* Sustainable Chemical Processes, 2013. **1**(1): p. 1-12.

16.   Lu, Y., et al., *Solid oxide fuel cell technology for sustainable development in China: An over-view.* international journal of hydrogen energy, 2018. **43**(28): p. 12870-12891.

17.   DING, Y.M., et al., *Electrooxidation Mechanism of Methanol at Pt-Ru Catalyst Modified GC Electrode in Electrolytes with Different pH Using Electrochemical and SERS Techniques.* Chinese Journal of Chemistry, 2007. **25**(11): p. 1617-1621.

18.   Gong, M. and H. Dai, *A mini review of NiFe-based materials as highly active oxygen evolution reaction electrocatalysts.* Nano Research, 2015. **8**: p. 23-39.

19.   Suen, N.-T., et al., *Electrocatalysis for the oxygen evolution reaction: recent development and future perspectives.* Chemical Society Reviews, 2017. **46**(2): p. 337-365.

20.   Hacquard, A., *Improving and understanding direct methanol fuel cell (DMFC) performance.* 2005.

21.   Anantharaj, S., et al., *Precision and correctness in the evaluation of electrocatalytic water splitting: revisiting activity parameters with a critical assessment.* Energy & Environmental Science, 2018. **11**(4): p. 744-771.

22. Hassan, A., et al., *Copper telluride nanowires for high performance electrocatalytic water oxidation in alkaline media.* Journal of Power Sources, 2021. **491**: p. 229628.

23. Görlin, M., et al., *Oxygen evolution reaction dynamics, faradaic charge efficiency, and the active metal redox states of Ni–Fe oxide water splitting electrocatalysts.* Journal of the American Chemical Society, 2016. **138**(17): p. 5603-5614.

24. Yu, F., et al., *Recent developments in earth-abundant and non-noble electrocatalysts for water electrolysis.* Materials Today Physics, 2018. **7**: p. 121-138.

25. Wu, L., et al., *Recent advances in self-supported layered double hydroxides for oxygen evolution reaction.* Research, 2020. **2020**.

26. Huang, X., et al., *Hierarchical iron-doped CoP heterostructures self-assembled on copper foam as a bifunctional electrocatalyst for efficient overall water splitting.* Journal of colloid and interface science, 2020. **569**: p. 140-149.

27. Li, X., et al., *Nanostructured catalysts for electrochemical water splitting: current state and prospects.* Journal of Materials Chemistry A, 2016. **4**(31): p. 11973-12000.

28. Jiao, Y., et al., *Design of electrocatalysts for oxygen-and hydrogen-involving energy conversion reactions.* Chemical Society Reviews, 2015. **44**(8): p. 2060-2086.

29. Shi, Y. and B. Zhang, *Recent advances in transition metal phosphide nanomaterials: synthesis and applications in hydrogen evolution reaction.* Chemical Society Reviews, 2016. **45**(6): p. 1529-1541.

30. Turner, J.A., *Sustainable hydrogen production.* Science, 2004. **305**(5686): p. 972-974.

31. Zhu, H., et al., *Atomic-scale core/shell structure engineering induces precise tensile strain to boost hydrogen evolution catalysis.* Advanced Materials, 2018. **30**(26): p. 1707301.

32. Chen, Z., et al., *Recent advances in transition metal-based electrocatalysts for alkaline hydrogen*

evolution. Journal of Materials Chemistry A, 2019. **7**(25): p. 14971-15005.

33. Li, F., et al., *Designed synthesis of multi-walled carbon nanotubes@ Cu@ MoS2 hybrid as advanced electrocatalyst for highly efficient hydrogen evolution reaction.* Journal of Power Sources, 2015. **300**: p. 301-308.

34. Lan, K., et al., *Ultrafine MoP nanoparticles well embedded in carbon nanosheets as electrocatalyst with high active site density for hydrogen evolution.* ChemElectroChem, 2018. **5**(16): p. 2256-2262.

35. Bandal, H.A., et al., *Bimetallic iron cobalt oxide self-supported on Ni-Foam: An efficient bifunctional electrocatalyst for oxygen and hydrogen evolution reaction.* Electrochimica Acta, 2017. **249**: p. 253-262.

36. Guo, X., et al., *Design and synthesis of CoFe2O4 quantum dots for high-performance supercapacitors.* Journal of Alloys and Compounds, 2018. **764**: p. 128-135.

37. Li, S., et al., *Bifunctional CoNi/CoFe 2 O 4/Ni foam electrodes for efficient overall water splitting at a high current density.* Journal of Materials Chemistry A, 2018. **6**(39): p. 19221-19230.

38. Li, Y., et al., *Direct chemical synthesis of ultrathin holey iron doped cobalt oxide nanosheets on nickel foam for oxygen evolution reaction.* Nano Energy, 2018. **54**: p. 238-250.

39. Ye, Z., et al., *Cobalt-iron oxide nanoarrays supported on carbon fiber paper with high stability for electrochemical oxygen evolution at large current densities.* ACS applied materials & interfaces, 2018. **10**(46): p. 39809-39818.

40. Chen, M., et al., *Cobalt (oxy) hydroxide nanosheet arrays with exceptional porosity and rich defects as a highly efficient oxygen evolution electrocatalyst under neutral conditions.* Journal of Materials Chemistry A, 2019. **7**(17): p. 10217-10224.

41. Babar, P., et al., *Cobalt iron hydroxide as a precious metal-free bifunctional electrocatalyst for*

efficient overall water splitting. Small, 2018. **14**(7): p. 1702568.

42. Liu, W., et al., *Amorphous cobalt–iron hydroxide nanosheet electrocatalyst for efficient electrochemical and photo-electrochemical oxygen evolution.* Advanced Functional Materials, 2017. **27**(14): p. 1603904.

43. Liu, Y., et al., *Small sized Fe–Co sulfide nanoclusters anchored on carbon for oxygen evolution.* Journal of Materials Chemistry A, 2019. **7**(26): p. 15851-15861.

44. Li, F., et al., *Synthesis of Cu–MoS2/rGO hybrid as non-noble metal electrocatalysts for the hydrogen evolution reaction.* Journal of Power Sources, 2015. **292**: p. 15-22.

45. Wang, K., et al., *Boosting hydrogen evolution via optimized hydrogen adsorption at the interface of CoP 3 and Ni 2 P.* Journal of Materials Chemistry A, 2018. **6**(14): p. 5560-5565.

46. Beltrán-Suito, R., P.W. Menezes, and M. Driess, *Amorphous outperforms crystalline nanomaterials: surface modifications of molecularly derived CoP electro (pre) catalysts for efficient water-splitting.* Journal of Materials Chemistry A, 2019. **7**(26): p. 15749-15756.

47. Danish, M.S.S., et al., *Photocatalytic applications of metal oxides for sustainable environmental remediation.* Metals, 2021. **11**(1): p. 80.

48. Wu, J., et al., *Co 3 O 4 nanocrystals on single-walled carbon nanotubes as a highly efficient oxygen-evolving catalyst.* Nano Research, 2012. **5**: p. 521-530.

49. Peng, L., et al., *Rationally design of monometallic NiO-Ni3S2/NF heteronanosheets as bifunctional electrocatalysts for overall water splitting.* Journal of Catalysis, 2019. **369**: p. 345-351.

50. Jiang, D., et al., *Synergistically integrating nickel porous nanosheets with 5d transition metal oxides enabling efficient electrocatalytic overall water splitting.* Inorganic Chemistry, 2021. **60**(11): p. 8189-8199.

51.   Sun, J., et al., *Cuprous sulfide derived CuO nanowires as effective electrocatalyst for oxygen evolution.* Applied Surface Science, 2021. **547**: p. 149235.

52.   Wu, X., et al., *NiCo/Ni/CuO nanosheets/nanowires on copper foam as an efficient and durable electrocatalyst for oxygen evolution reaction.* International Journal of Hydrogen Energy, 2020. **45**(41): p. 21354-21363.

53.   Zhang, T., et al., *Binder-free bifunctional SnFe sulfide/oxyhydroxide heterostructure electrocatalysts for overall water splitting.* International Journal of Hydrogen Energy, 2023. **48**(12): p. 4594-4602.

54.   Li, T., et al., *Crystalline nickel sulfide integrated with amorphous cobalt sulfide as an efficient bifunctional electrocatalyst for water splitting.* International Journal of Hydrogen Energy, 2023. **48**(20): p. 7337-7345.

55.   Zhang, H., et al., *Engineering heterostructure of bimetallic nickel-silver sulfide as an efficient electrocatalyst for overall water splitting in alkaline media.* Journal of Solid State Chemistry, 2022. **316**: p. 123556.

56.   Fan, H., et al., *Facile one-step electrodeposition of two-dimensional nickel-iron bimetallic sulfides for efficient electrocatalytic oxygen evolution.* Journal of Alloys and Compounds, 2022. **894**: p. 162533.

57.   Pattanayak, P., et al., *Fabrication of cost-effective non-noble metal supported on conducting polymer composite such as copper/polypyrrole graphene oxide (Cu2O/PPy–GO) as an anode catalyst for methanol oxidation in DMFC.* international journal of hydrogen energy, 2018. **43**(25): p. 11505-11519.

58.   Wang, Y., X. Wang, and C.M. Li, *Electrocatalysis of Pd–Co supported on carbon black or ball-milled carbon nanotubes towards methanol oxidation in alkaline media.* Applied Catalysis B:

Environmental, 2010. **99**(1-2): p. 229-234.

59.   Li, B., et al., *Highly active Pt–Ru nanowire network catalysts for the methanol oxidation reaction.* Catalysis Communications, 2012. **18**: p. 51-54.

60.   Asadi, F., S.N. Azizi, and S. Ghasemi, *A novel non-precious catalyst containing transition metal in nanoporous cobalt based metal-organic framework (ZIF-67) for electrooxidation of methanol.* Journal of Electroanalytical Chemistry, 2019. **847**: p. 113181.

61.   Raoof, J.B., R. Ojani, and S.R. Hosseini, *An electrochemical investigation of methanol oxidation on nickel hydroxide nanoparticles.* South African Journal of Chemistry, 2013. **66**: p. 47-53.

62.   Das, A.K., et al., *Reduced graphene oxide (RGO)-supported NiCo 2 O 4 nanoparticles: an electrocatalyst for methanol oxidation.* Nanoscale, 2014. **6**(18): p. 10657-10665.

63.   Li, X., et al., *Enhanced activity and durability of platinum anode catalyst by the modification of cobalt phosphide for direct methanol fuel cells.* Electrochimica acta, 2015. **185**: p. 178-183.

64.   Candelaria, S.L., et al., *Multi-component Fe–Ni hydroxide nanocatalyst for oxygen evolution and methanol oxidation reactions under alkaline conditions.* ACS Catalysis, 2017. **7**(1): p. 365-379.

65.   Mehek, R., et al., *Novel Co-MOF/graphene oxide electrocatalyst for methanol oxidation.* Electrochimica Acta, 2017. **255**: p. 195-204.

66.   Li, X., et al., *Electrochemical fabrication of ultra-low loading Pt decorated porous nickel frameworks as efficient catalysts for methanol electrooxidation in alkaline medium.* Journal of Power Sources, 2018. **396**: p. 64-72.

67.   Guerrero-Ortega, L., et al., *Methanol electro-oxidation reaction at the interface of (bi)-metallic (PtNi) synthesized nanoparticles supported on carbon Vulcan.* International Journal of Hydrogen Energy, 2018. **43**(12): p. 6117-6130.

68.   Chen, L., et al., *CuO/Co (OH) 2 nanosheets: a novel kind of electrocatalyst for highly efficient*

electrochemical oxidation of methanol. ACS applied materials & interfaces, 2018. **10**(45): p. 39002-39008.

69.   Askari, M.B., et al., *One-step hydrothermal synthesis of MoNiCoS nanocomposite hybridized with graphene oxide as a high-performance nanocatalyst toward methanol oxidation.* Chemical Physics Letters, 2018. **706**: p. 164-169.

70.   Noor, T., et al., *A highly efficient and stable copper BTC metal organic framework derived electrocatalyst for oxidation of methanol in DMFC application.* Catalysis Letters, 2019. **149**: p. 3312-3327.

71.   Wu, Y.P., et al., *Bi-Microporous metal–organic frameworks with cubane [M4 (OH) 4](M= Ni, Co) clusters and pore-space partition for electrocatalytic methanol oxidation reaction.* Angewandte Chemie International Edition, 2019. **58**(35): p. 12185-12189.

72.   Wojtyła, S. and T. Baran, *Copper-nickel-oxide nanomaterial for photoelectrochemical hydrogen evolution and photocatalytic degradation of volatile organic compounds.* Materials Research Bulletin, 2021. **142**: p. 111418.

73.   Hamnett, A., *Mechanism and electrocatalysis in the direct methanol fuel cell.* Catalysis today, 1997. **38**(4): p. 445-457.

74.   Wang, J., et al., *Recent progress in cobalt-based heterogeneous catalysts for electrochemical water splitting.* Advanced materials, 2016. **28**(2): p. 215-230.

75.   Wang, X., et al., *Intensified Kirkendall effect assisted construction of double-shell hollow Cu-doped CoP nanoparticles anchored by carbon arrays for water splitting.* Applied Catalysis B: Environmental, 2023. **325**: p. 122295.

76.   Yang, X., et al., *Interface reinforced 2D/2D heterostructure of Cu-Co oxides/FeCo hydroxides as monolithic multifunctional catalysts for rechargeable/flexible zinc-air batteries and self-powered*

water splitting. Applied Catalysis B: Environmental, 2023. **325**: p. 122332.

77.   Jia, J., et al., *Understanding the growth of NiSe nanoparticles on reduced graphene oxide as efficient electrocatalysts for methanol oxidation reaction.* Ceramics International, 2020. **46**(8): p. 10023-10028.